Structural, dynamic, electronic, and vibrational properties of flexible, intermediate, and stressed rigid As-Se glasses and liquids from first principles molecular dynamics

M. Bauchy, A. Kachmar, and M. Micoulaut

Citation: The Journal of Chemical Physics **141**, 194506 (2014); doi: 10.1063/1.4901515
View online: http://dx.doi.org/10.1063/1.4901515
View Table of Contents: http://scitation.aip.org/content/aip/journal/jcp/141/19?ver=pdfcov
Published by the AIP Publishing

Structural, dynamic, electronic, and vibrational properties of flexible, intermediate, and stressed rigid As-Se glasses and liquids from first principles molecular dynamics

M. Bauchy,[1] A. Kachmar,[2,3] and M. Micoulaut[2,a)]
[1]*Department of Civil and Environmental Engineering, University of California, Los Angeles, California 90095-1593, USA*
[2]*Laboratoire de Physique Théorique de la Matière Condensée, Université Pierre et Marie Curie, 4 Place Jussieu, F-75252 Paris Cedex 05, France*
[3]*Qatar Environment and Energy Research Institute, Qatar Foundation, P.O. Box 5825, Doha, Qatar*

(Received 19 September 2014; accepted 31 October 2014; published online 20 November 2014)

The structural, vibrational, electronic, and dynamic properties of amorphous and liquid As_xSe_{1-x} ($0.10 < x < 0.45$) are studied by First Principles Molecular Dynamics. Within the above range of compositions, thresholds, and anomalies are found in the behavior of reciprocal and real space properties that can be correlated to the experimental location of the Boolchand intermediate phase in these glassy networks, observed at $0.27 < x < 0.37$. These findings are associated with diffusion anomalies for the parent liquid phase, thereby linking structural and dynamical atomic-scale fingerprints for the onset of rigidity within the network, while also providing a much more complex picture than the one derived from mean-field approaches of stiffness transitions. © *2014 AIP Publishing LLC*. [http://dx.doi.org/10.1063/1.4901515]

I. INTRODUCTION

Arsenic selenides (As–Se) are typical semiconductors, and form covalent network glasses over a wide range in composition from melt quench. They are used as starting materials in bulk or thin film form, and serve for the design of a certain number of promising optoelectronic applications.[1–4] As a result, the number of studies under various conditions and forms have increased substantially in the recent years[5–7] with special emphasis on the giant photoplasticity that is typical of these materials.

The molecular structure of As_xSe_{1-x} glasses in the chalcogen rich region (x < 40% As) has been described in the early literature[8–11] as a random network of pyramidal $AsSe_{3/2}$ units that cross-link the base Se chain structure when the As content is increased. Support for the pyramidal local structure in glasses and liquids have been obtained from neutron,[12–18] X-ray diffraction,[19–24] extended absorption x-ray diffraction[25–29] (EXAFS), anomalous X-ray scattering,[30,31] and Nuclear Magnetic Resonance (NMR).[32–35] In addition, Raman spectroscopy,[36–46] infrared absorbance[9,37,40,47–49] have shown that the spectrum of elemental Se which consists of several modes typical of Se–Se bond vibrations is affected as the As content is changed. New peaks associated with the formation of pyramidal $AsSe_{3/2}$ units appear, and these seem to indicate that the addition of As proceeds in a stochastic fashion for compositions lower than ≃15%, whereas a non-stochastic addition sets in for larger As content. This change in régime has been already noticed in an early study of As-Se glasses.[50] In chalcogenides, given the weaker chemical bond strength between species, there is an increased tendency to find chemical disorder which manifests by the presence of homopolar bonds in the corresponding stoichiometric compound.[51–53] These features can be also found in the As_2Se_3 glass.[54,55] Renninger and Averbach[23] noticed that the first and second neighbor peaks of the measured rdf at 40% and 50% As are qualitatively similar to those obtained from the crystals As_2Se_3[56] and As_4Se_4,[57] the latter containing homopolar As–As bonds. This might indicate the presence of such motifs, maybe even before the stoichiometric composition of As_2Se_3.

The increased interest in performing systematic studies of As-Se glasses, including the present numerical one, is also driven by recent experimental findings[58,59] in the context of flexible to rigid transitions.[60–62] According to the seminal work of Phillips[63] and Thorpe,[64] a flexible to rigid transition is achieved when a glass network constrained by bond-stretching and bond-bending forces reaches the critical network mean coordination number of $\bar{r} = 2.4$ at which an isostatic stress-free glass network is obtained. This mean-field condition seems to be fulfilled in the As–Se binary at the composition of 40% As where anomalies in glass transition temperature and mechanical properties have been reported. In fact, if one assumes that the atoms obey the 8-$\mathcal{N}$ rule ($\mathcal{N}$ being the number of s and p electrons), and that As and Se are, respectively, in three- and twofold coordination, one has $\bar{r} = xn_{As} + (1-x)n_{Se}x = 2 + x$. This leads to the anticipated threshold of $x = 40\%$ As and $\bar{r} = 2.4$ at the stoichiometric composition As_2Se_3. Given the elastic nature of the predicted threshold[63,64] and the connection with optimal glass formation,[65] a certain number of experimental studies have focused either on the enthalpic properties at the glass transition[45,58,59,66–70] including under ageing,[71,72] or on elastic properties,[73–75] thermal transport,[76,77] and viscosity.[78–82]

However, this traditional picture has been challenged recently. First, evidence for a double transition/threshold

a)mmi@lptl.jussieu.fr

(x_{c1}, x_{c2}) has been reported instead of the single one at x_c = 40% As,[58,59] and also evidenced in the isovalent As_xS_{1-x}.[83] This defines for the As_xSe_{1-x} glasses a compositional window $x_{c1} < x < x_{c2}$ that has been indentified with an intermediate phase (IP), bounded by a chalcogen-rich phase with low network connectivity ($x < x_{c1}$) and an As-rich phase ($x > x_{c2}$) which is overconstrained or stressed rigid. In contrast with other investigated systems however, the IP boundaries of the As–Se binary appear to be less well defined.[58] In the IP, glasses usually display some remarkable properties such as low internal stress[84] that leads to weak ageing phenomena,[85] minimal enthalpic changes at the glass transition,[86–91] space-filling tendencies,[92–94] and super-strong glass-forming melts leading to a low fragility index m.[95,96] IP properties appear to be generic because they are now observed in many other simple or multicomponent oxide[97–100] and chalcogenide glasses,[101–103] or even in complex materials including proteins[104] or hydrogenated SiC thin films.[105] These generic IP features have been recovered for the case of As_xSe_{1-x} glass. Weaker ageing phenomena[106] in the $x_{c1} < x < x_{c2}$ range have been reported (as compared to the flexible and stressed rigid phase), as well as calorimetric windows[58,59] (Fig. 1), fragility minima[81,82,107] (Fig. 1, right axis), and space-filling tendencies.[107] The observation of these spectacular changes occurring within the $x_{c1} < x < x_{c2}$ range requires special care in sample preparation because it has been shown that measurements are highly sensitive to dryness or homogeneity.[107,109,110] As an unfortunate consequence, there have been reported statements challenging[82,111,112] the existence of the intermediate phase. However, measurements leading to such contradicting conclusions have been made on samples of unproven homogeneity as recently demonstrated.[59,107,108] Previous theories of the flexible to rigidity transition have been modified in order to take into account the observed phenomena, and have arrived to the conclusion that the IP may result from the self-organization of the network[113–118] which becomes rigid but adapts under increasing stress $x > x_{c1}$, while delaying percolation of stressed rigidity up to the second threshold x_{c2}.[119]

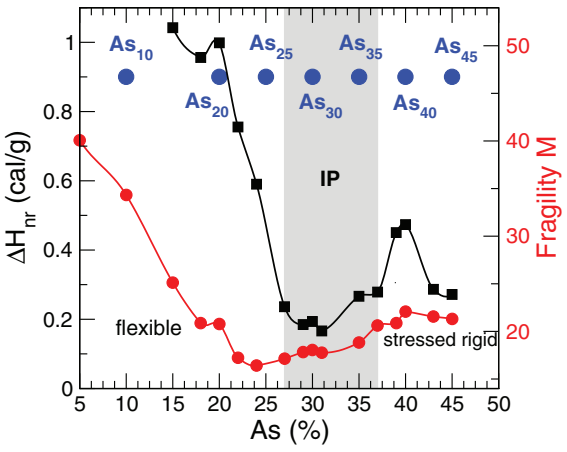

FIG. 1. Anomalous behaviour of physical quantities of As_xSe_{1-x} glasses across the intermediate phase (taken from Refs. 96 and 107): Non-reversing heat flow $\Delta H_{nr}(x)$ (black curve) and fragility index m (red curve, right axis). The present investigated systems by First Principles Molecular Dynamics (FPMD) are shown in blue: $As_{10}Se_{90}$, $As_{20}Se_{80}$, $As_{25}Se_{75}$, $As_{30}Se_{70}$, $As_{35}Se_{65}$, $As_{40}Se_{60}$ (As_2Se_3), and $As_{45}Se_{55}$.

In the As-Se glasses (but also in As-S), additional structural information have emerged from the discovery of the IP. The location of both the rigidity (x_{c1}) and stress transition (x_{c2}) have been found to be shifted[58,59] to lower As composition, with a window roughly determined at 27% $\simeq x_{c1} < x < x_{c2} \simeq$ 37% (Fig. 1), i.e., lower than the predicted mean-field threshold of x_c = 40%. To account for this shift, it has been proposed that isostatic quasi-tetrahedral (QT) Se = $AsSe_{3/2}$ units should exist in the glass, given that these QTs correspond to a stoichiometry of As_2Se_5 (x = 28.5%). Such units are found in corresponding phosphorus based glasses,[120] and have been also used to interpret vibrational and photoelectron spectroscopic measurements[121] of As_2S_5, and used subsequently for the analysis of As-Se glasses.[122] An argument on the $T_g(x)$ variation in As–Se has led to a rough estimate of 30% QT units.[58] However, no direct experimental evidence has been found from Raman[46] or Nuclear Quadrupole Resonance[123] except in thin films produced by flash evaporation. Luksha *et al.*[124] have analyzed, indeed, the radial distribution function of such obtained amorphous structures, and have indicated that the flash evaporation temperatures which are relatively higher than conventional evaporation methods may promote the formation of such local structures involving a subsequent electronic hybridization necessary for the As=Se double bonding. The existence of QT units appears, thus, to be strongly tied to temperature and to the way melts are quenched to the glass, consistent with recent Molecular Dynamics studies[55,125] showing that fourfold arsenic does exist in the liquid state, and represent the dominant structural motif at elevated temperatures. Nevertheless, there have been theoretical[30,126] investigations indicating that QT units might be also present in the glass, and the results seem to agree with those obtained experimentally from anomalous X-ray scattering.[31,127]

Given these different open issues regarding structure but also dynamics, we report in the present contribution on a systematic investigation with composition of As_xSe_{1-x} glasses and liquids using First-Principles Molecular Dynamics (FPMD) simulations. We concentrate on seven target compositions spanning over the flexible, intermediate, and stressed rigid phase (10 $\leq$ x $\leq$45% As), and on the structural, electronic, vibrational and dynamic properties. There have been a quite important body of studies on the simulation of As-Se glasses, most of them being focused on the stoichiometric As_2Se_3. Classical molecular dynamics simulations with a 3-body force field has been used to obtain the atomic structure of different As-Se glasses.[126] *Ab initio* or FPMD methods using density functional theory (DFT) have been used to study the structural and electronic properties[30,54,55,128–130] at selected compositions (As_2Se_3, AsSe), light induced changes[131–133] and effect of irradiation.[134] Using similar tools, liquid As-Se have been also investigated as a function of temperature[125] to determine the origin of the semi-conductor to metal transition, and the relationship to structure.[135,136]

In the present contribution, results of the investigation on As_xSe_{1-x} show an agreement of unprecedented quality

for both the structure factor and the pair correlation function when these functions are compared to experimental counterparts. In real space, although the total pair correlation function $g(r)$ does not evolve much with As content, the increase of x leads to important changes in partial structure. Homopolar As–As bonding detected from the partial As–As pair correlation function grow, indeed, substantially for $x \geq 35\%$ As, and a continuous decrease of Se–Se bonds is obtained. As a consequence of these two opposite trends, the number of heteropolar As–Se bonds is found to be maximum for the intermediate phase compositions. In reciprocal space, the calculated structure factor is found to be in excellent agreement with various experimental data from neutron or X-ray diffraction. An analysis of the partials shows that signatures of intermediate range order exhibit an anomalous behavior in the IP that leads to non-monotonic trends in composition for the parameters characterizing the first sharp diffraction peak (FSDP). We analyze the electronic (electronic density of states, EDOS) and vibrational properties (vibrational density of states, VDOS) and the topology of the networks (coordination numbers, angles, bondings pairs, rings). Finally, we investigate the liquid phase, and find that IP melts display a maximum in diffusivity while also displaying an increased ease to diffusion which manifests by a minimum in the corresponding activation energy for diffusion. An additional analysis arises from the calculation of Van Hove correlation functions. Taken together, these results provide a first systematic plane wave DFT study with composition across the stiffness transitions, and effects of the flexible to rigid transitions are evidenced from various structural and dynamic properties. The paper is organized as follows. In Sec. II we detail the DFT scheme used for the simulations, and present in Secs. III and IV the structural results in reciprocal and real space, respectively. Section V is then devoted to the detail of the network topology and its change with As content. Section VI describes the electronic and vibrational properties and their evolution with As content. Finally, Sec. VII presents the dynamic behavior in the liquid phase.

II. COMPUTATIONAL DETAILS

First principles molecular dynamics simulations[137,138] have been performed on As_xSe_{1-x} systems containing $N = 200$ atoms at seven different compositions (10%, 20%, 25%, 30%, 35%, 40%, 45% As) with the number of atoms being given by $N_{As} = xN$ and $N_{Se} = (1 - x)N$. At a first glance, the spacing of the chosen compositions may be seen as rather coarse to detect the transitions into and out the IP. However, one has to keep in mind that the size of systems does not permit to investigate tiny compositional changes given that a change of 1% As will involve a change of 2 atoms, only, which would lead, we believe, to results of unsufficient statistical accuracy. A periodically repeated cubic cell was used, whose size changes according to the compositionnaly dependent number density of the glass[58] (e.g., 18.06 Å for the 20% As, Fig. 2). For the simulation of the present As-Se glasses and liquids, we use DFT in combination with plane wave basis sets. The electronic scheme has been chosen after a series of methodological investigations on different liquid and amorphous chalcogenides (Ge–Se) showing that (i) a generalized gradient approximation (GGA) for the exchange-correlation energy improves substantially[139] the description of both short and intermediated range order in liquid $GeSe_2$ as compared to the local density approximation (LDA), (ii) an alternative exchange-correlation functional[53,140] (with respect to Ref. 139), derived after PW Becke (B) for the exchange energy[141] and Lee, Yang, and Parr (LYP) for the correlation energy[142] leads to a structure with a reduced number of miscoordinated atoms and metallic character, and improves the reproduction of vibrational spectra[143] or NMR properties.[144]

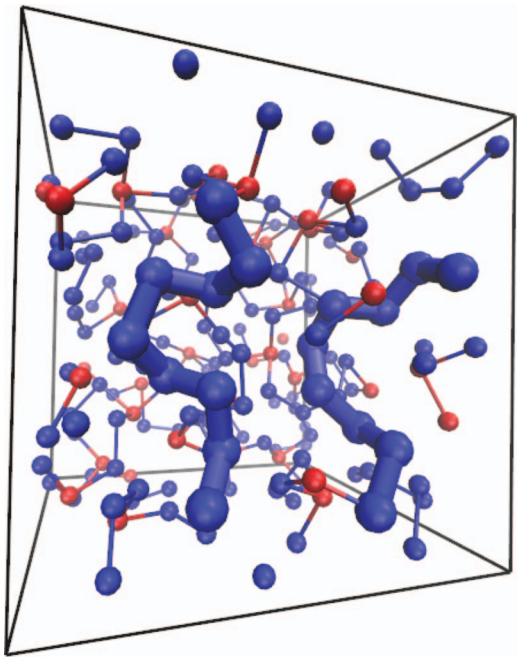

FIG. 2. A snapshot of amorphous $As_{20}Se_{80}$ containing Se (blue) and As atoms (red). The system still contains fragments (highlighted) of the chain structure typical of amorphous selenium.

Using these results, the electronic structure of the As-Se liquids and glasses was described within DFT and evolved self-consistently during the motion using a GGA for the exchange and correlation parts of the total energy, according to Becke (B) and LYP, respectively.[141,142] Valence electrons were treated explicitly, in conjunction with normconserving pseudopotentials to account for core-valence interactions. The wave functions were expanded at the Γ point of the supercell and the energy cutoff was set at 20 Ry. Starting configurations represent a random structure of As and Se atoms fulfilling the desired stoichiometry, and the loss of the memory of the initial configurations has been achieved through preliminary runs at 2000 K over 50 ps. For all compositions and temperatures, statistical averages in the liquid state were obtained over 25 ps of trajectory with a time step of $\Delta t = 0.12$ fs and a fictitious mass of 200 a.u. At 1200 K, three uncorrelated configurations separated by 5 ps have been selected to provide starting sets of coordinates for a quenching schedule (T = 800 K, T = 600 K) aimed at the obtention of an amorphous system at T = 300 K.

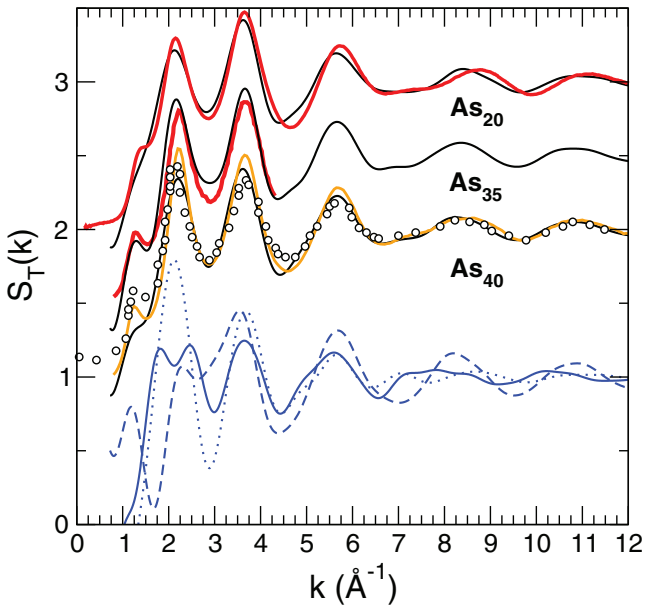

FIG. 3. Total simulated structure factor $S_T(k)$ of amorphous $As_{20}Se_{80}$, $As_{35}Se_{65}$ (compared to experimental $As_{33}Se_{67}$), and $As_{40}Se_{60}$ (top, black solid lines) compared to experimental data from Bychkov *et al.*[22] (red curves), Fabian *et al.*[13] (circles), and Xin and Salmon[14] (orange curve). A decomposition into partial structure factors is shown for As_{40} (As_2Se_3, blue curves): As–As (solid curve), As–Se (broken curve), Se–Se (dotted curve).

III. RECIPROCAL SPACE PROPERTIES

A. Total structure factors

In Fig. 3 the total structure factors $S_T(k)$ for amorphous $As_{20}Se_{80}$, $As_{35}Se_{65}$, and $As_{40}Se_{60}$ are represented and compared to the most recent experimental data.[13,14,22] The agreement between experiments and simulation appears to be excellent over all wavevectors for the stoichiometric composition (40% As). The two principal peaks at $k_{PP1} = 2.2$ Å^{-1} and $k_{PP2} = 3.7$ Å^{-1} are very well reproduced, and also the peaks at higher k ($k > 6$ Å). For the lower compositions (20% and 35% As), the agreement with experimental data is even better. Note that the FSDP, while rather small in experiments,[14] reduces in the simulations to a simple shoulder on the low wavevector side of the main peak, especially for the $As_{40}Se_{60}$ (As_2Se_3) composition, but it is entirely reproduced for $As_{35}Se_{65}$.

B. Partial structure factors

We are not aware of a full resolution of partial structure factors from isotopic substituted neutron diffraction as for the case of $GeSe_2$,[51] and therefore rely on a partial resolution that has been reported from anomalous X-ray scattering.[31,127] Fig. 4 shows the simulated partial differential structure factors $\Delta_{As}S(k)$ and $\Delta_{Se}S(k)$ compared to experimental data from anomalous X-ray scattering[31] in glassy As_2Se_3. Once again, the agreement is very good, and demonstrates the ability of the present simulation to provide a realistic description of both As and Se environment. As observed in simulation as well as in experiment, only $\Delta_{As}S(k)$ shows a FSDP at $k \simeq 1.2$ Å^{-1}, which suggests that correlations in the medium range order (i.e., at low k) mainly arise from As atoms. This is also evidenced from the full analysis of the Faber-Ziman partial

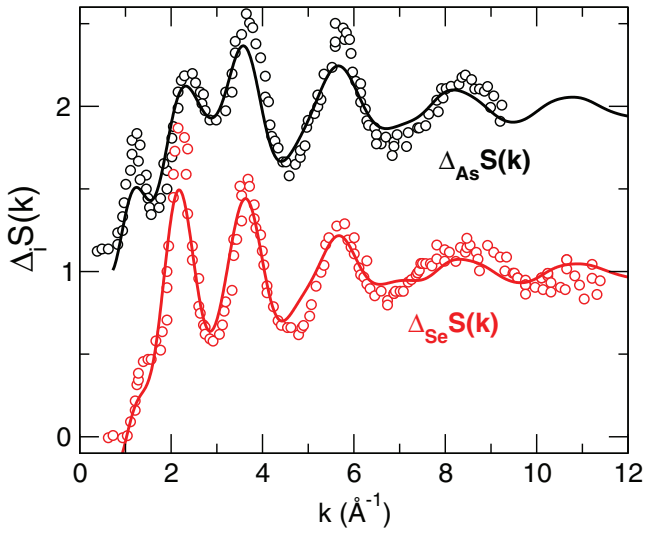

FIG. 4. Simulated partial differential structure factors $\Delta_i S(k)$ (solid lines) compared to experimental data (circles) from anomalous X-ray scattering[31] in glassy $As_{40}Se_{60}$.

structure factors shown in Fig. 3 for As_2Se_3 (blue curves), and in Fig. 5 for the different selected compositions.

This decomposition into partial structure factors indicates that a FSDP is, indeed, present in $S_{AsSe}(k)$ but not in $S_{AsAs}(k)$ and indicates the dominant contribution to the FSDP found in $\Delta_{As}S(k)$. On the other hand, $S_{SeSe}(k)$ mostly contributes to the principal peaks at $k_{PP1} = 2.2$ Å^{-1} and $k_{PP2} = 3.7$ Å^{-1}, and represents with $S_{AsSe}(k)$ the dominant contribution to $S_T(k)$. Given the neutron coherent scattering lengths of the chemical species $b_{As} = 6.58$ fm and $b_{Se} = 7.97$ fm and the range of considered compositions, the contribution of $S_{AsAs}(k)$ to the main peak in $S_T(k)$ is, indeed, limited to less than 10%, because one has for instance for $x = 30\%$:

$$S_T(k) = 0.066 S_{AsAs}(k) + 0.375 S_{AsSe}(k) + 0.559 S_{SeSe}(k). \quad (1)$$

Although no clear evolution in the partial structure factor are observed with As content, we can note that the intensity of the main peak at $k_{PP1} \simeq 2.2$ Å^{-1} increases with As content, a feature indicating that the structure evolves towards a As_2Se_3-like one, with a dominant peak at k_{PP1} for the 40% As composition. Simultaneously, Se–Se correlations build up at distances of about $7.7/k_{PP1} = 3.5$ Å.[145] The FSDP observed in $S_{AsSe}(k)$ deserves a more careful study as detailed next.

C. Evidence for thresholds and anomalies

In order to better characterize the FSDP, a Lorentzian fit (red curves in Fig. 5) is used in order to extract its paramaters (Table I) among which the position k_{FSDP} and width Δk_{FSDP} as a function of As content, used in:

$$S_{FSDP}(k) = I_0(x) + \frac{I_{FSDP}}{1 + \left(\frac{k - k_{FSDP}}{\Delta k_{FSDP}/2}\right)^2}. \quad (2)$$

As displayed in Fig. 6, the position k_{FSDP} decreases from 1.25 Å^{-1} to 1.17 Å^{-1} between 20% and 40% As.

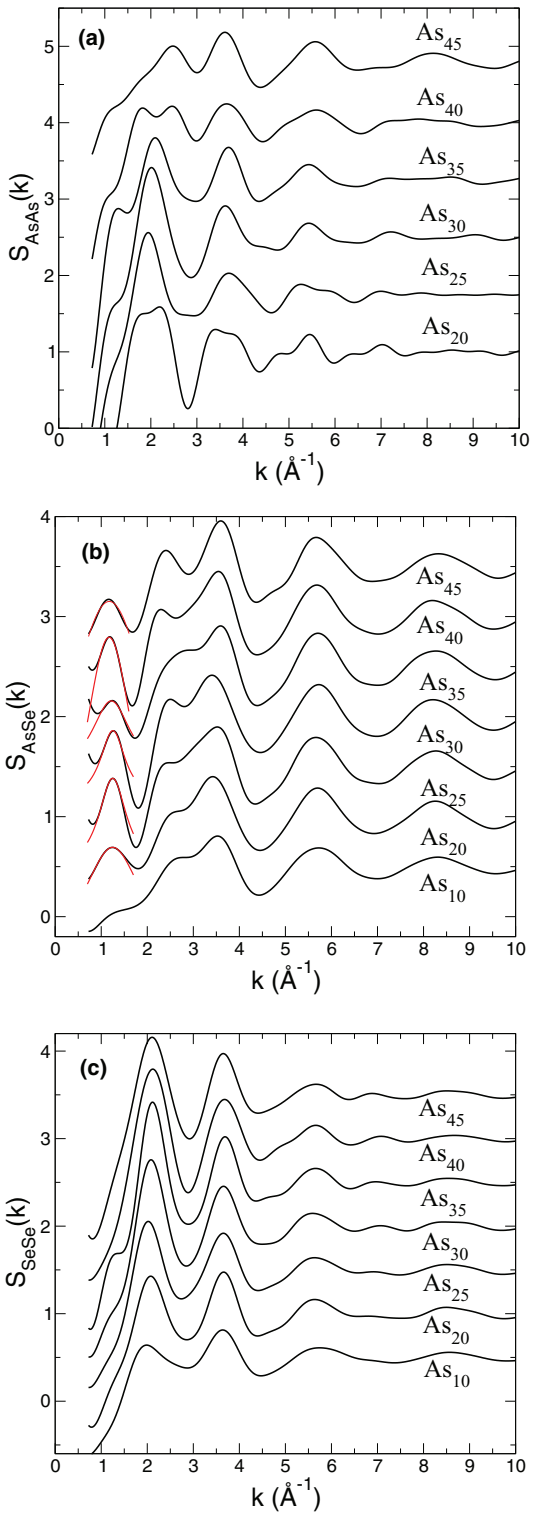

FIG. 5. Computed Faber-Ziman partial structure factor $S_{ij}(k)$ as a function of composition x in As_xSe_{1-x} glasses. Red curves in panel b represent Lorentzian fits (Eq. (2)) to the FSDP in $S_{AsSe}(k)$ (see also Table I).

Furthermore, while the FSDP position k_{FSDP} remains nearly constant in the flexible phase at low As content ($x < 30\%$), it drops at the approximate boundary of the rigidity transition, found experimentally at 27%–29% As.[58,107] This behavior on the partial $S_{AsSe}(k)$ contrasts with the one found for the total $S_T(k)$ for which no such threshold behavior is found.[22] Interestingly, the intensity and width of the FSDP show a minimum in the IP (30% As, Table I and Fig. 6). Since the position of the FSDP reflects some repetitive characteristic distance between structural units, results of Fig. 6 suggest that in the flexible phase (x <29%) a typical lengthscale of distance $L = 7.7/k_{FSDP} \simeq 6.2$ Å builds up for the As–Se correlations with decreasing As content. In microcrystals, the width of the Bragg diffracting peaks is directly related to the average size of microcrystals, following the well-known Scherrer equation.[146] This leads to the definition of a correlation length defined by $\xi = 7.7/\Delta k_{FSDP}$ which increases from x = 4.7 Å to 11.5 Å from $As_{20}Se_{80}$ to $As_{30}Se_{70}$, and then decreases with growing As content. It indicates that the observed minimum in Δk_{FSDP} of Fig. 6 is correlated with the emergence of a typical lengthscale ξ that characterizes the IP given that ξ becomes maximum in the range where the experimental signature[58,107] of the IP has been detected (Fig. 1).

TABLE I. Parameters of the Lorentzian fit (red curves in Fig. 5) of the FSDP in the partial structure factor $S_{AsSe}(k)$: y-position I_0 with respect to the baseline at $k \to \infty$, intensity I_{FSDP}, peak position k_{FSDP}, full width at half maximum Δk_{FSDP}.

	I_0	I_{FSDP}	k_{FSDP} (Å^{-1})	Δk_{FSDP} (Å^{-1})
$As_{20}Se_{80}$	− 0.240(4)	0.927(2)	1.248(3)	1.649(3)
$As_{25}Se_{75}$	0.439(9)	0.942(4)	1.249(2)	0.751(7)
$As_{30}Se_{70}$	1.159(5)	0.698(8)	1.252(6)	0.671(9)
$As_{35}Se_{65}$	1.303(9)	0.856(2)	1.217(2)	1.057(2)
$As_{40}Se_{60}$	0.796(5)	1.973(3)	1.171(0)	1.475(0)
$As_{45}Se_{55}$	− 1.670(2)	4.821(2)	1.175(2)	1.609(4)

In addition, one must stress that our findings on As–Se for both k_{FSDP} and Δk_{FSDP} have a one to one correspondence with results[147] obtained from a systematic study on a different glass system where rigidity is tuned by pressure. Here the same FSDP anomalies are also located in an intermediate phase (a pressure window[147,148]), underscoring therefore not only the generic behavior of such trends but also the fact that there is clearly a structural signature for the IP, a conclusion that contrasts with previous negative conclusions on a similar system (Ge–Se[149]). In the present As–Se binary, isotopic substituted neutron diffraction measurements as a function of As content would provide a direct access to the partial structure factor $S_{AsSe}(k)$. At this stage however, only the anomalous X-ray diffraction experiment of Hosokawa *et al.*[31] have

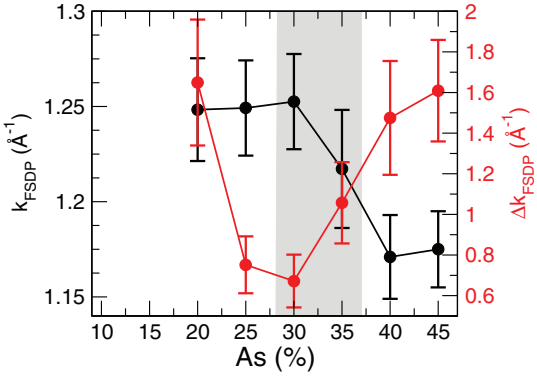

FIG. 6. Position k_{FSDP} and width Δk_{FSDP} (red curve, right axis) of the As–Se FSDP as a function of composition. The gray zone indicates the rigid intermediate phase, determined experimentally.[58,107]

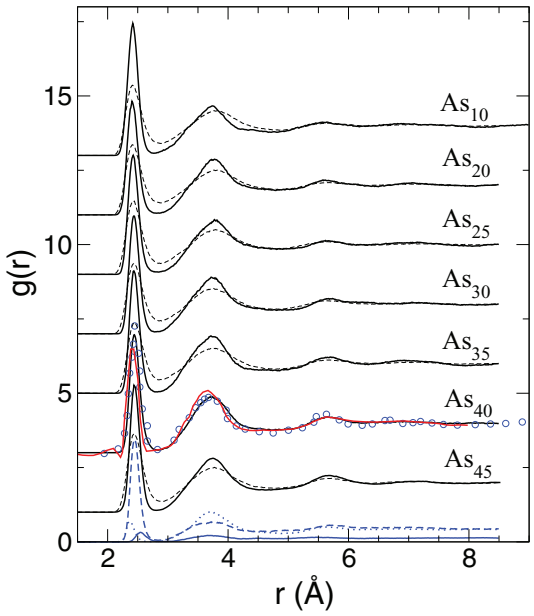

FIG. 7. Calculated total pair correlation function $g(r)$ for As_xSe_{1-x} glasses (black curves), and compared to available experimental data (circles, Fabian *et al.*;[13] red curve, Xin *et al.*[14]). The blue curves represent the decomposition into partial pair correlation functions $g_{ij}(r)$ for the As_{40} (As_2Se_3) compound: As–As (solid curve), As–Se (broken curve), and Se–Se (dotted curve). Broken curves correspond to the calculated total pair correlation function at 800 K (see text for details).

led to a partial information on a single composition (As_2Se_3, Fig. 4). The experimental partial differential function $\Delta_{As}S(k)$ displays a position $k_{FSDP} = 1.23$ Å^{-1} which is in excellent agreement with our calculations (Table I and Fig. 4).

IV. REAL SPACE PROPERTIES

A. Pair correlation functions

The total pair correlation function $g(r)$ is represented in Fig. 7 for the glasses with varying As content. For the composition at which experimental data is available[13,14] (As_2Se_3), an excellent agreement is found and all typical features of the function g(r) are reproduced: position, width and intensity of the principal peak at $r = d_1$ defining the first correlation or bond distance, and the secondary peak at $r = d_2$ (Table II). We notice a slight overestimation of the bond distances when compared to experimental findings.[14,23,26] The peak positions are found to increase moderately with As content as d_1 changes from 2.41 Å for $As_{20}Se_{80}$ to 2.44 Å for $As_{45}Se_{55}$ (Table II), qualitatively consistent with findings from EXAFS[26] showing an increase from 2.38 to 2.41 Å between the 20% and the 40% (As_2Se_3) composition. However, on the overall, it is clearly evidenced that, obviously, the global shape of the pair correlation function does not change much with As content (Fig. 7). On the opposite, it is found that the position of the secondary peak at d_2 decreases with As content. However, while the peak at d_1 is mostly due to As–Se correlations (blue curves in Fig. 7) and does not vary much with x, the secondary peak at $\simeq 3.7$ Å results from contributions arising from all pairs (As–As, As–Se, and Se–Se, see below) which do evolve with composition.

TABLE II. Calculated structural properties of As_xSe_{1-x} glasses with varying As content: Calculated d_i first ($i = 1$) and second ($i = 2$) neighbour peak positions (in Å) of the total $g(r)$ and partial pair correlation function $g_{ij}(r)$, together with obtained first minimum r_m of each $g_{ij}(r)$, and corresponding calculated coordination numbers n_{ij}. The calculated distances are compared to measured ones from neutron,[14] X-ray[23] and EXAFS.[26] Note that experimental compositions may differ by 1 at. %.

		d_1 (Å)	d_2 (Å)	r_m (Å)	n_{ij}
$\mathbf{As_{10}Se_{90}}$	Total	2.43	3.76		
	As–As	...	3.75	...	...
	As–Se	2.43	3.71	2.80	2.76
	Se–Se	2.37	3.78	2.80	1.70
$\mathbf{As_{20}Se_{80}}$	Total	2.41	3.77		
		2.38[23,26]	3.69[23]		
	As–As	2.59	3.82	2.87	0.05
	As–Se	2.47	3.72	2.87	2.96
	Se–Se	2.39	3.74	2.80	1.27
$\mathbf{As_{25}Se_{75}}$	Total	2.43	3.77		
		2.38[23]	3.68[23]		
		2.39[26]			
	As–As	2.54	3.79	2.90	0.08
	As–Se	2.46	3.79	2.87	2.94
	Se–Se	2.39	3.79	2.77	1.03
$\mathbf{As_{30}Se_{70}}$	Total	2.43	3.72		
		2.40[23]	3.66[23]		
		2.39[26]			
	As–As	2.57	3.70	2.92	0.07
	As–Se	2.47	3.70	2.82	2.94
	Se–Se	2.39	3.73	2.77	0.74
$\mathbf{As_{35}Se_{65}}$	Total	2.43	3.71		
		2.41[23]	3.65[23]		
		2.40[26]			
	As–As	2.53	3.82	2.94	0.37
	As–Se	2.46	3.72	2.89	2.66
	Se–Se	2.41	3.71	2.79	0.59
$\mathbf{As_{40}Se_{60}}$	Total	2.44	3.71		
		2.39[14]	3.62[14]		
		2.40[23]	3.68[23]		
		2.41[26]			
	As–As	2.55	3.67	2.98	0.65
	As–Se	2.45	3.75	2.87	2.40
	Se–Se	2.37	3.70	2.67	0.42
$\mathbf{As_{45}Se_{55}}$	Total	2.44	3.71		
	As–As	2.51	3.73	2.84	1.14
	As–Se	2.44	3.70	2.79	1.85
	Se–Se	2.39	3.75	2.74	0.48

Fig. 8 shows the behavior of the partial pair correlation functions $g_{ij}(r)$ (As–As, As–Se, and Se–Se) with corresponding principal peak (PP) distances d_1 and d_2 given in Table II. The pair distribution function $g_{AsSe}(r)$ does not vary much with increasing As content (Fig. 8(b)), and remains dominated by the intense first peak at $d_1 \simeq 2.46$ Å corresponding to the As–Se bond length (experimentally, $\simeq$2.41 Å[26]). A secondary peak builds up with growing x, and it can be associated with distances involving the two adjacent $AsSe_{3/2}$ motifs. An inspection of the total $g(r)$ and the decomposition into partials (blue curves, Fig. 7) shows that g_{AsSe} represents the dominant contribution to the total pair correlation function $g(r)$ and to

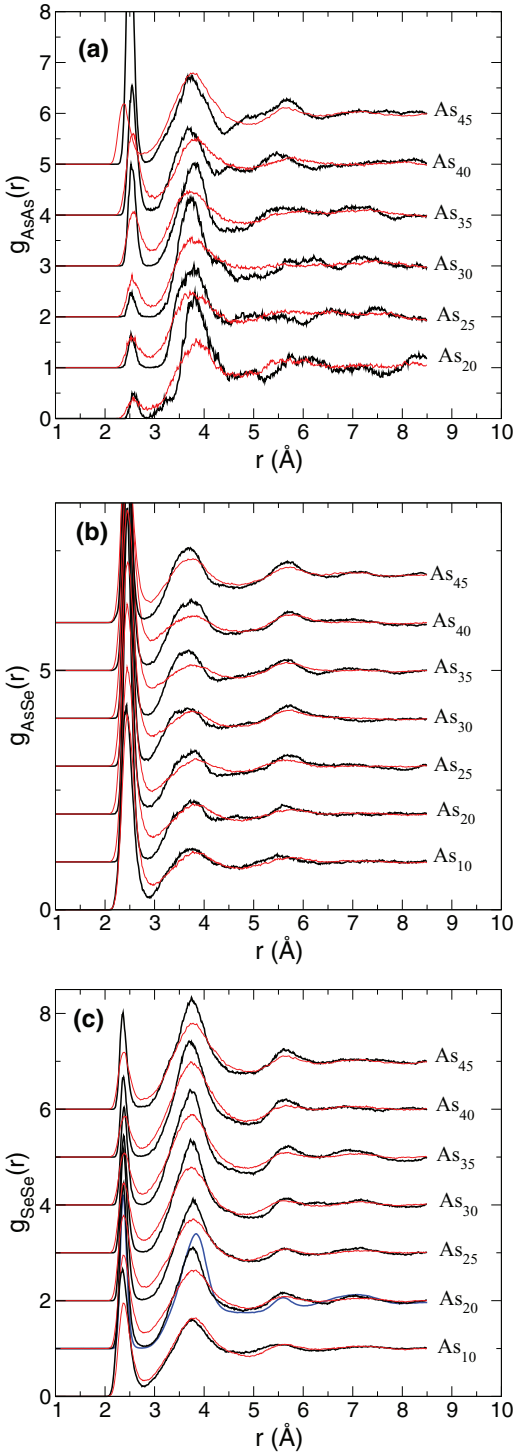

FIG. 8. (a)–(c) Computed pair distribution functions g_{ij} (i, j = As, Se) as a function of composition x in As_xSe_{1-x} glasses. The blue curve corresponds to the pair correlation function g_{SeSe} of $Ge_{20}Se_{80}$ and serves for comparison.[152] Red curves are the corresponding pair correlation functions $g_{ij}(r)$ in liquid As–Se (800 K). See text for details.

the PP at $r = d_1$. Furthermore, it is seen that the first distances As–As and Se–Se represent the high- and low-r tail of this PP, respectively. In fact, for As_2Se_3, the PP is found at $d_1 = 2.44$ Å (Table II) for the total $g(r)$ and has a main contribution from As–Se (2.45 Å), but also minor contributions from Se–Se (2.37 Å) and As–As (2.55 Å).

The two other pair correlation functions (Se–Se and especially As–As) indicate that the real space correlations display a threshold behavior close to the IP compositions, as seen from Figs. 8(a) and 8(c). The pre-peaks at 2.55 Å and 2.37 Å are identified with homopolar As–As and Se–Se bondings, respectively, the Se–Se peak position corresponding to the bond length of the base selenium glass.[150,151] As expected, the intensity of this Se–Se pre-peak decreases with increasing amount of As since the length of Se chains tends to decrease. The intensity of the secondary peak at ≃3.74 Å (in, e.g., $As_{20}Se_{80}$) increases with As content, but the underlying structural mechanism leading to this trend is more subtle as recently shown for the case of Ge–Se glasses.[152] In Se-rich glasses, the secondary peak results from Se–Se interchain and second chain neighbor correlations at 3.75 Å.[151] These contributions decrease with growing As content because of the reduction of the Se chain length, and because of the progressive As-driven cross-linking of the polymeric chain network that is typical of vitreous selenium.[150] However, with the growing presence of arsenic, the Se–Se distance defining the edge of the $AsSe_{3/2}$ pyramid (found at a similar distance of 3.70 Å) becomes progressively the dominant contribution of this secondary peak.

On the contrary, the intensity of the As–As pre-peak found at 2.55–2.59 Å increases with As content. For the selenium-rich compositions and up to 35% As, the intensity of this pre-peak is nearly constant (about 0.5) but then grows substantially to ≃2 and ≃6.5 for $As_{35}Se_{65}$ and $As_{40}Se_{60}$, respectively. For the latter, this pre-peak is even more intense than the PP found at 3.67 Å and associated with two connected $AsSe_{3/2}$ motifs. These trends suggest that important changes take place in the network structure close to the stressed rigid phase as an important growth of homopolar bondings is obtained.

The integration of the different partial structure factors (Fig. 8) leads to an estimate of the As and Se coordination numbers as a function of As content. We integrate each function $g_{ij}(r)$ up to its first minimum r_m (Table II) and obtain the partial coordination numbers n_{AsAs}, n_{AsSe}, and n_{SeSe} as a function of As content. Note that one has $(1 - x)n_{SeAs} = xn_{AsSe}$. Results are given in Table II. The important growth of As–As bonds at 35% is also acknowledged by an important increase of n_{AsAs} which evolves from 0.05 to 1.14 between the 20% and the 45% As composition. On the opposite, a decrease of the Se–Se partial coordination number is found, consistent with the reduction of the Se–Se pairs in the network structure.

Total coordination numbers $n_{As} = n_{AsAs} + n_{AsSe}$ and $n_{Se} = n_{SeSe} + n_{SeAs}$ are found to follow very closely the 8-$\mathcal{N}$ rule, as it is found on average for nearly all compositions $n_{As} \simeq 3$ and $n_{Se} \simeq 2$, consistent with investigations of the real space structure using, e.g., neutron diffraction.[12–18] The increase of As–As bonds for compositions larger than 35% As tends to reduce the contribution of n_{AsSe} at the expense of n_{AsAs} but on the overall the $n_{As} \simeq 3$ is maintained. n_{As} is found to vary indeed between 3.01 and 3.05 between the two ends of the investigated compositional range. At a global level, one can thus conclude on the validity of a glass structure made of threefold coordinated As atoms which cross-link a base Se network made of twofold selenium atoms.

TABLE III. Proportion of the different coordination units in glassy As–Se systems for the seven compositions of interest. The cut-off distances for the calculation of the coordination numbers have been taken at the minimum of the pair distribution functions ($r_m = 2.87$ Å). The population of tetrahedral As determined from BB enumeration (see Sec. V B) are also given.

	$As_{10}Se_{90}$	$As_{20}Se_{80}$	$As_{25}Se_{75}$	$As_{30}Se_{70}$	$As_{35}Se_{65}$	$As_{40}Se_{60}$	$As_{45}Se_{55}$
As^{II}	0.9	0.2	0.2	0.2	0.1	0.7	1.3
As^{III}	84.4	94.3	92.8	91.2	94.3	89.6	90.6
As^{IV}	13.7	5.4	6.7	7.8	5.5	9.2	8.0
As^{IV} from Sec. V B 2	0.2	5.5	5.6	7.6	6.4	10.0	1.6
As^{V}	0.9	0.1	0.3	0.8	0.1	0.5	...
Se^{I}	9.5	5.9	4.5	4.2	3.5	5.0	3.6
Se^{II}	88.9	93.5	95.1	95.2	95.6	93.9	95.1
Se^{III}	1.5	0.6	0.4	0.6	0.9	1.1	1.3
$\bar{r}_{As}$	3.14	3.05	3.07	3.09	3.06	3.10	3.14
$\bar{r}_{Se}$	1.91	1.95	1.96	1.96	1.97	1.96	1.97
$\bar{r}$	2.04	2.17	2.24	2.30	2.35	2.41	2.50

V. NETWORK TOPOLOGY

A. Coordination numbers

The analysis of the distribution of r-coordinated species confirms what has been obtained (n_{ij}) from the integration of the partial par correlation function, i.e., one has a majority of 2-fold selenium (Se^{II}) and 3-fold arsenic (As^{III}, Table III). At the stoichiometric composition, 3-fold As represent ≃90% of all As atoms, whereas 93.9% Se atoms are twofold coordinated. This rate does not vary much with composition as one finds in $As_{20}Se_{80}$ 94.3% and 93.5% for As^{III} and Se^{II}, respectively. Coordination defects essentially arise from 4-fold As which represents 6%–9% for all compositions, whereas 1-fold (terminal) Se has smaller amounts (4%–6%). As a result, the averaged coordination numbers $\bar{r}_{As}$ and $\bar{r}_{Se}$ are close to the estimate from the pair correlation functions (Table II). Finally, the network mean coordination number $\bar{r}$ is found to follow what would be anticipated from a simple use of the 8-$\mathcal{N}$ rule, i.e., $\bar{r} = 2(1 - x)+3x = 2+x$, i.e., one has $\bar{r} = 2.35$ for the $As_{35}Se_{65}$ composition (Table III). As mentioned above, it has been proposed[121] that QT units may exist in As-Se glasses, and their existence has been invoked[58] to account for the evolution of the glass transition temperature with As content, and with the shift of the intermediate phase to the Se-rich domain. Given our results, the presence of such QT units appears to be rather unlikely at ambient temperature given the weak fraction (5%–10%, Table III) which is also consistent with an estimate (7%) from an independent *ab initio* simulation,[30] but Reverse Monte carlo simulations fitted to diffraction results lead to an increased fraction (25%).

B. Nature of QT units

Using the simulated trajectories of the various As-Se glasses, we calculate the fraction and the nature of such possible QT units with composition and temperature using a topological analysis based on constraints.

1. Defining a tetrahedra

Instead of working on the angles which are typical of the pyramidal (98°[31]) and tetrahedral (109°) geometry but too close to be separated from a global bond angle distribution (see below), we use constraint counting algorithms that have been recently introduced.[153–155] We analyze the angular excursions around a central atom because a tetrahedron is defined by six rigid angles or $n_c^{BB} = (2r - 3) = 5$ independent constraints[63,64] (the sixth angle is determined from the five independent ones). During the simulation trajectory and after having defined a set of N neighbors around a central As atom, each of the N_a=N(N-1)/2 angles is then followed individually.[153] This defines a bond-angle distribution P(θ) which can be characterized by a mean $\bar{\theta}$ and a standard deviation σ_θ, which represents the second moment of P(θ).

When the number of low standard deviations σ_θ around an atom is six, six rigid angles are detected and an As tetrahedra is identified. Once the analysis is performed over the whole system and system averages are realized, one has a precise fraction η_T of tetrahedra as a function of composition. Figure 9 shows the results of such an analysis by representing the system averaged standard deviation $\langle\sigma_\theta\rangle$ for amorphous $As_{30}Se_{70}$. It can be noticed that a certain number of As atoms display, indeed, six angles with a low standard deviation (red bars, $_1As_2$, $_1As_3$, $_1As_4$, ..., $_3As_4$), typically $\langle\sigma_\theta\rangle \simeq 10°$, i.e., much lower than the other values resulting from angles involving the second nearest neighbors of the As atom (e.g., angle numbers 4, 5, 8, 9, ...) which have a $\langle\sigma_\theta\rangle$ about four times larger. Once the six angular excursions are identified, Figure 9(b) shows indeed that the associated system-averaged mean angle is equal to $\langle\bar{\theta}\rangle \simeq 105°$–$109°$ (red arrows), and a corresponding bond angle distribution (Fig. 9(c)) peaks at 109°. The remaining atoms which contribute to the dominant pyramidal geometry display, as expected, a bond angle distribution centred at 98° (green curve in Fig. 9(c)), and one also has $\langle\bar{\theta}\rangle \simeq 98°$ for the relevant angles having a rigid angular constraint (green arrows in Fig. 9(b)).

2. Behavior of QT with composition

Having established the fraction of QT units, we study their population as a function of composition and temperature. Table III shows such trends, and it is found that such QT units represent in glasses only a small fraction

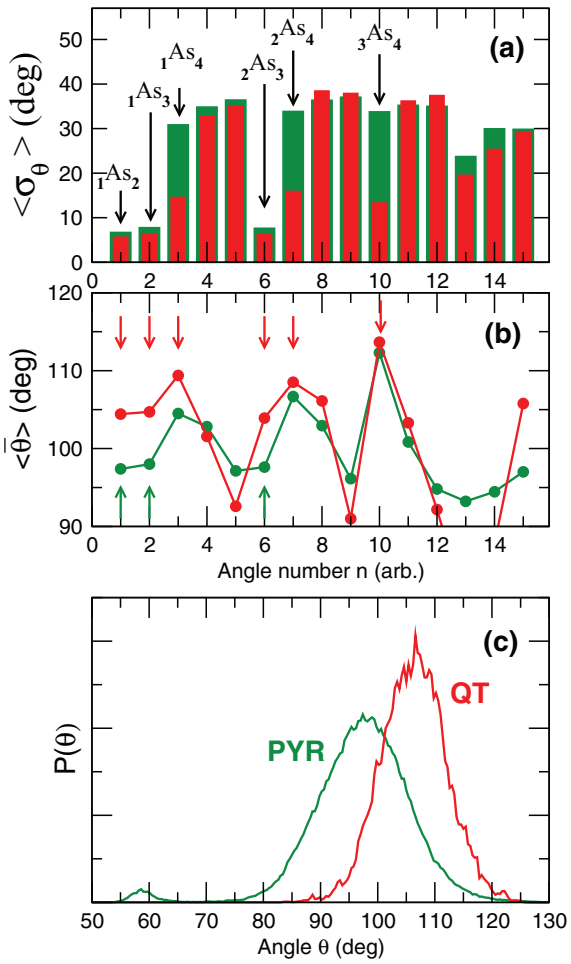

FIG. 9. (a) Standard deviation $\langle\sigma_\theta\rangle$ for arbitrary angle numbers n ($0< n<N_a = 15$) around As atoms in amorphous $As_{30}Se_{70}$ split into two categories: As atoms having 6 low σ_θ's (red bars), and As atoms having not such six σ_θ's (green bars) and which represent the dominant pyramidal $AsSe_{3/2}$ geometry. The arrows indicate the relevant angles $_kAs_m(n)$ serving for the discussion. Here m and $k < m$ are the neighbors of As, and labelled according to their distance with respect to the central As atom. (b) Corresponding As-centred angles $\langle\bar{\theta}\rangle$. Colored arrows indicate angles which can be considered as rigid (because of panel (a)) and which serve to cross-check the angles ($\simeq$109° or $\simeq$98°) of the local geometries. (c) Bond angle distribution of identified tetrahedral (QT, red curve)/pyramidal (PYR, green curve) As.

($\eta_T \simeq 10\%$), certainly lower that the proposed fraction of 30% necessary to account for both the shift of the intermediate phase to lower connectivities ($\bar{r} < 2.4$) with respect to the mean-field result,[64] and the evolution of the glass transition temperature at low As content.[58]

This is, again, also consistent with our neighbor distribution decomposition of the partial pair correlation function $g_{As}(r)$ showing that only the first three neighbor distributions contribute to the peak, whereas the fourth one is only present at the first minimum r_m of $g_{As}(r)$, and contributes only marginally to the integral of $4\pi r^2 g_{As}(r)$, i.e., to n_{As}.

However, it has been found[54] that the fraction η_T of tetrahedra increases substantially with temperature, this feature being true for all investigated compositions. In the stoichiometric As_2Se_3, a sharp increase of four-fold As between 600 K and 1000 K is obtained, i.e., close to the glass transition region (468 K[58]), but this is also observed for other compositions, and even for the Se-rich ones ($As_{20}Se_{80}$). The presence of QT units may thus be strongly dependent on the thermal conditions of glass synthesis with probable important effects arising from the cooling rate dependence and from ageing. Furthermore, since QT units are dominant at elevated temperatures, hyperquenched glasses may possibly reveal an increased fraction of such geometries, as speculated from results on flash evaporation experiments.[124]

C. Bonding pairs

We now compute the statistical fraction of bonding pairs p_{ij} from the simulation, and results are shown in Fig. 10(a). Se–Se bonds decrease in a monotonic fashion as the As content is increases, and this contrasts with the statistics of As–As bonds displaying an obvious threshold behavior at 30% As. The fraction p_{AsAs} of homopolar bonding then increases dramatically, and the threshold is found to coincide with the chalcogen-rich boundary of the intermediate phase. These trends can actually be recovered qualitatively from the intensity of the pre-peak at $\simeq$2.5 Å of the As–As partial pair correlation functions (Fig. 8), which shows an increase in intensity, once $x \geq 30\%$ As.

These features appear to be hardly detectable from an analysis of the total pair distribution function (Fig. 7) given the small contributions of such As–As pairs to the first peak which is mostly due to to As–Se correlations. The combination of both trends, p_{SeSe} and p_{AsAs}, leads to a non-monotonic behavior for heteropolar bonds in the intermediate phase (Fig. 10(b)) which is maximum for the intermediate phase composition $x = 30\%$.

Relative concentrations of bonding pairs can usually be simply described by two sets of models. In a first model (random covalent network, RCN[156,157]), the bond statistics is just given by a random distribution with probability $p_{ij}^{RCN} \propto \mathcal{W}_{ij} x_i x_j$ where x_i and x_j (i,j = As,Se) are the concentrations of the species As or Se, and $\mathcal{W}_{ij} = (2-\delta_{ij}) n_i n_j$ is a statistical factor involving the coordination numbers n_i, and represents the number of equivalent ways to connect two (As, Se) species together. δ_{ij} is the Kronecker symbol. With a normalization condition $\sum_{i,j} p_{ij}^{RCN} = 1$, one has, e.g.:

$$p_{AsAs}^{RCN} = \frac{9x^2}{\bar{r}^{\,2}}, \tag{3}$$

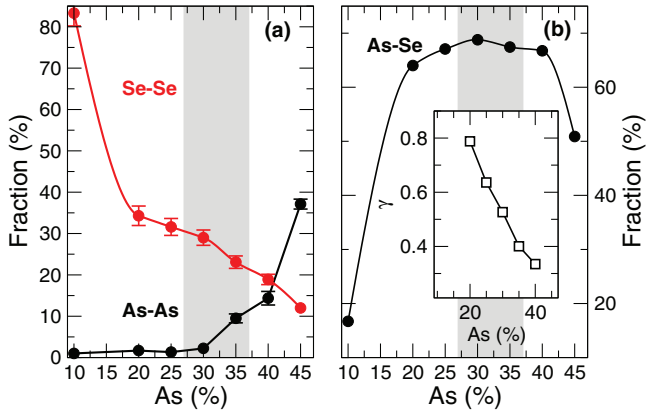

FIG. 10. Computed statistics p_{ij} of homopolar (a) and heteropolar (b) bonds in As_xSe_{1-x} glasses for different As content. The inset represents the degree of chemical order γ as a function of As content (see text for details).

$$p_{AsSe}^{RCN} = \frac{12x(1-x)}{\bar{r}^{\,2}}, \tag{4}$$

$$p_{SeSe}^{RCN} = \frac{4(1-x)^2}{\bar{r}^{\,2}}. \tag{5}$$

An alternative model, the chemically ordered (CON) one,[156,158,159] suggests that only As–Se and Se–Se bonds are possible in the chalcogen-rich (x<40%) region, and $p_{AsSe} = 1$ for $As_{40}Se_{60}$ so that homopolar As–As bonds can only appear at larger compositions. For $x < 40\%$, the probability of finding an $AsSe_{3/2}$ structure is given by $2x/(2-3x)$, and the bond probabilities lead to:

$$p_{AsSe}^{CON} = \frac{12x}{2+7x}, \tag{6}$$

$$p_{SeSe}^{CON} = \frac{2-5x}{2+7x}. \tag{7}$$

Both statistics are obviously unable to account for the trends obtained in Fig. 10 given that p_{AsSe}^{CON} steadily increases from zero at $x = 0$ to one for As_2Se_3. In addition, one obviously does not have a fully heteropolar network at the stoichiometric composition (which contradicts the CON model), and neither the threshold behavior for As–As bonds, nor the maximum in As–Se at 30% As can be described using the RCN model (Fig. 10).

Building on an approach which has been introduced by Fee and Trodhal,[160] we define the degree of chemical order γ of the glass by

$$p_{ij}(\gamma) = \gamma p_{ij}^{CON} + (1-\gamma)p_{ij}^{RCN}. \tag{8}$$

Using the equations above, we can evaluate the network tendency to be in either a chemically ordered or random situation by following γ as a function of As content, having at our disposal the computed bond statistics p_{AsSe} from the simulated trajectories (Eq. (8)). Results (inset of Fig. 10(b)) now show that, on a global level, the network tends to evolve from a chemically ordered network into a random network because γ continuously decreases from values of about $\simeq$0.8 down to 0.3, i.e., with now a more prominent contribution from the RCN bond distributions. This trend is not very surprising. At low content there is a zero probability to have As–As bonds so that the tendency to have each As surrounded by three Se atoms is at its maximum, thus fulfilling the CON picture. However, it is worth to remark that none of the detected anomalies at intermediate phase compositions (threshold in As–As bond statistics, maximum in As–Se) can be reproduced from these simple minded approaches.

D. Bond angle distribution

Fig. 11 shows the relevant bond angle distributions of As-Se glasses as a function of As content. One notices that the Se–As–Se bond angle distribution is centred at an angle of $\simeq$98° indicative of the pyramidal geometry, and consistent with the estimate from anomalous X-ray scattering[31] and with Fig. 9. This distribution appears to be weakly dependent on the As content, in contrast with some of the other distributions. Angles involving a central selenium are highly dependent of the nature of the neighboring atoms. Indeed, while

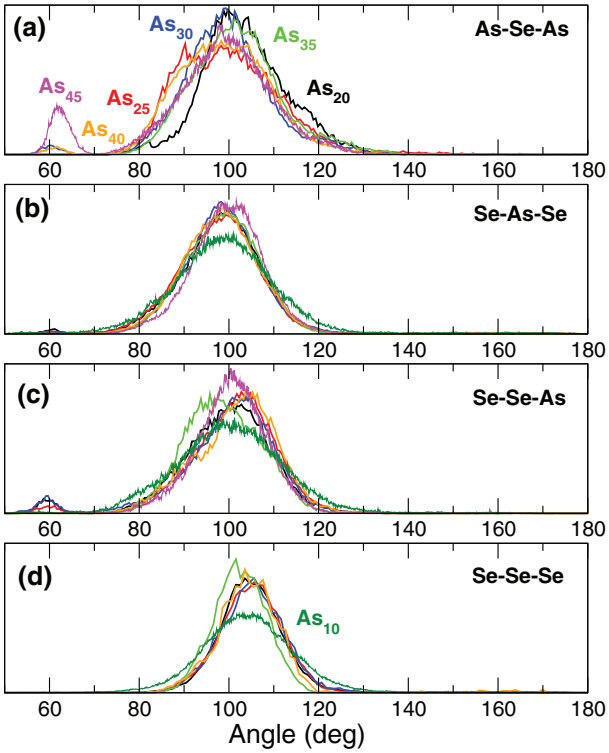

FIG. 11. Computed As–Se–As (a), Se–As–Se (b), Se–Se–As (c), and Se–Se–Se (d) bond angle distribution in As_xSe_{1-x} glasses for different As content. These distributions have been calculated by including neighbors separated by less than 2.9 Å.

the Se–Se–Se distribution (Fig. 11(d)) is weakly dependent on the As composition, the presence of As leads to distributions which evolve with composition, as highlighted for the As–Se–As distribution, and, to a lesser extent, for the Se–Se–As one (Figs. 11(a) and 11(c)). The presence of two As neighboring atoms leads to a substantial broadening of the Se-centred angle and to a slight shift of the mean angle. Indeed, for $As_{20}Se_{80}$ we find $\theta \simeq 100°$ and $\simeq 104°$ for As–Se–As and Se–Se–Se, respectively. Finally, we note that the $As_{35}Se_{65}$ composition (green curves) differs slightly from the other compositions with a reduced mean angle for Se–Se–As and Se–Se–Se triplets (Fig. 11(c)).

Next, we also consider the variation of the dihedral angle $\bar{\delta}$ with As content (Fig. 12). It is found that with increasing x, the dihedral angle decreases from values of about 88° for $As_{10}Se_{90}$ to 70° for the 45% As composition (Fig. 10(b)). For the IP compositions, small changes are obtained and $\bar{\delta}$ remains nearly constant between 30% and 35% As. The decrease of the dihedral angle reflects in some way the global stiffening of the network structure with the growing presence of As cross-links, and is consistent with previous results found for Ge-Se glasses for which a similar trend was obtained[154] as the system moved from the flexible to the stressed rigid phase. However, values for $\bar{\delta}$ were found to be substantially lower ($\simeq$30°–35°) indicating a more compact structure. The angular excursion of the dihedral angle characterized by the second moment σ_δ of the angular distribution shows exactly the opposite behavior, i.e., σ_δ increases for $x > 20\%$ As (Fig. 10(b), right axis) and this may indicate that under

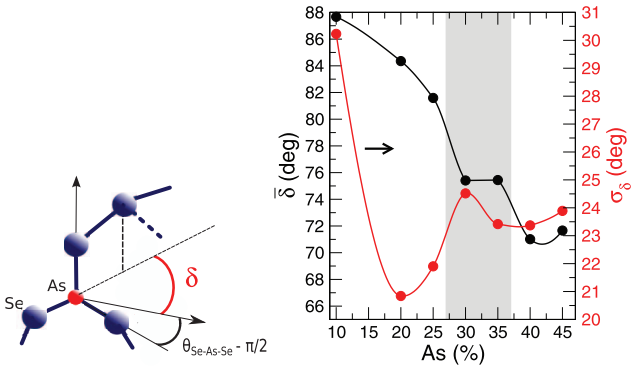

FIG. 12. (Left) Definition of the dihedral angle δ. Note that the upper blue atom can be also an arsenic atom. (Right) Behavior of the mean dihedral angle $\bar{\delta}$ and corresponding standard deviation σ_δ (red curve, right axis) in As_xSe_{1-x} glasses as a function of As content. The gray zone represents the experimentally reported IP.[58,107]

increasing stress, angles adapt by experiencing a larger torsional motion.

E. Ring statistics

Aspects of topological intermediate range order can be characterized from the investigation of the ring statistics. We have applied for all investigated compositions an algorithm that is mostly based on the King[161]-Franzblau[162] shortest path search, and which is now part of the Rigorous Investigation of Networks Generated using Simulation (RINGS) code.[163] The statistics is computed up to rings of size $n = 14$, and a cutoff distance of 2.9 Å has been used for all atomic pairs (As−As, As−Se, and Se−Se), which nearly corresponds to the minimum of the pair correlation function. Note that results are not affected by a change of ±0.1 Å.

Figure 13 shows the ring statistics $R^{(n)}$ for the seven compositions. First, it is important to emphasize that, in contrast with oxide glasses (SiO_2, GeO_2) having 100% heteropolar bonds and only even sized rings,[164,165] chalcogenides can have both even and odd sized rings because of the presence of homopolar bonds. The presence of such odd rings is also an indication for the presence of As–As and Se–Se bonds, whereas even rings can be be either fully heteropolar or contain some homopolar bonds, the former being known in the literature as ABAB alternation structured rings.[166]

For the stoichiometric composition (x = 40%), we recover a situation previously encountered[152] in $GeSe_2$, i.e., one notes (Fig. 13) the presence of homopolar As–As or Se–Se bonds which allows the possibility to have closed loops of odd size. For $As_{40}Se_{60}$, the ring structure is dominated by small rings of size $3 \leq n \leq 6$ (Fig. 14), and some larger rings ($n \geq 10$) are also found in the network.

When followed with As content, it is found at a global level that the increase of x tends to increase the number of possible ring structures as evidenced by the small number of rings ($R^{(n)} \simeq$ 2-3) for $As_{10}Se_{90}$ or $As_{20}Se_{80}$. This is essentially due to the chain-like nature of the Se-rich network which does not permit to form small or intermediate sized rings while leaving the possibility to have some larger rings made of long Se chains (see Fig. 2). Some $n = 7$ rings emerge from the enumeration, however. An additional search of rings of sizes having $n \geq 14$ shows that $As_{20}Se_{80}$ also contains loops with 20 atoms of more. We find that the intermediate phase compositions $As_{30}Se_{70}$ and $As_{35}Se_{65}$ exhibit an increased tendency to form rings of intermediate sizes ($7 \leq n \leq 10$), but an increase in composition promotes small rings ($n \leq 7$, see also Fig. 14), or even larger rings that are also possible given the increased bonding possibilities as the cross-linking density is increased. These non-monotonic trends may be put in parallel with the non-monotonic evolution in bonding pairs (As–As, As–Se, and Se–Se, Fig. 10) which must affect the way rings organize during the formation of the glass. The population of these small rings tends to grow even more as the As content is increased to 40% or 45%. Interestingly, when the ABAB analysis is performed (i.e., a search for fully heteropolar rings), the odd rings tend to be nearly 100% heteropolar, and do not contain any homopolar Se–Se or As–As bonds.

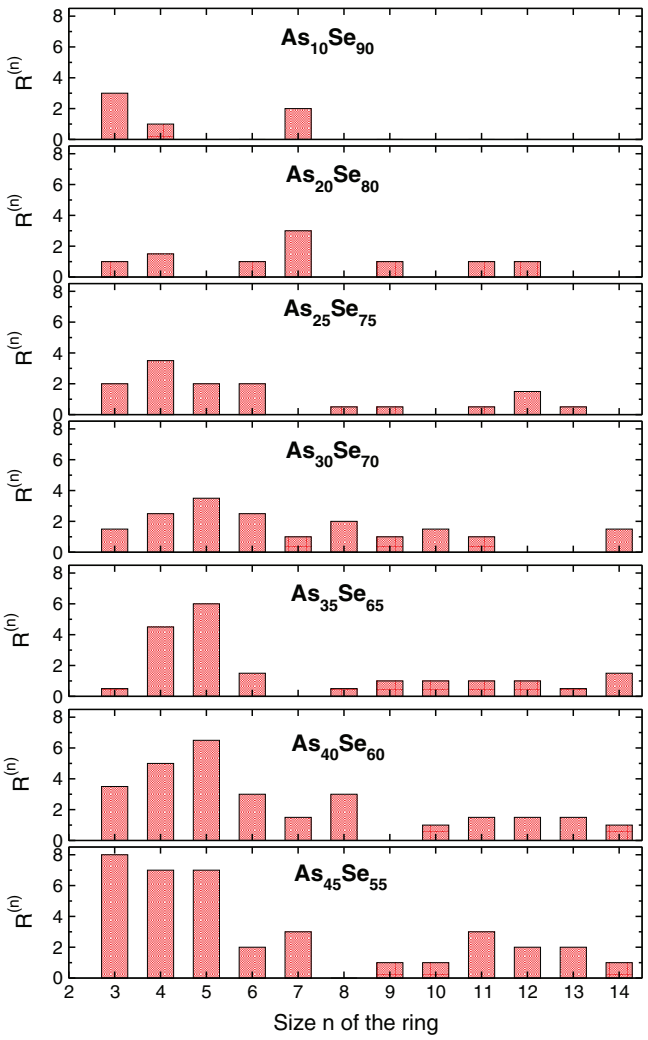

FIG. 13. Calculated number of rings $R^{(n)}$ in amorphous As_xSe_{1-x} for different As content using the RINGS method.[163]

In itself, the present analysis also indicate the difference in topology that is found when the As–Se system is compared to the Ge-Se glass[152] (Fig. 15). For the latter, the fraction of small rings has been found to increase more rapidly when the density of cross-links (Ge) increases. The ring density is

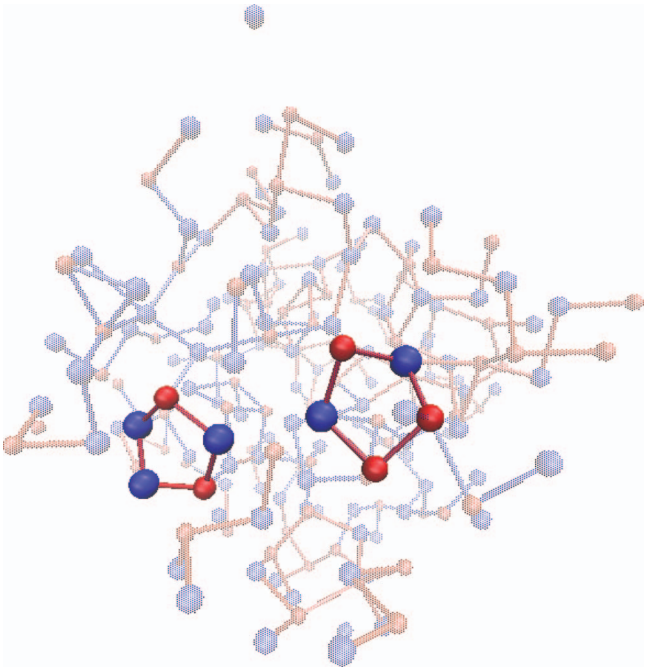

FIG. 14. Two typical 5-fold ring structures in glassy $As_{40}Se_{60}$ containing either a homopolar As–As or a Se–Se bond.

also found to be substantially higher when compared to the present As–Se system. Furthermore, no threshold behavior is obtained in the As-Se glasses, a situation that also contrasts with the one determined in the Ge–Se system for which, obviously, the small ring density increases at the intermediate to stressed rigid boundary (Fig. 15(a)).

VI. ELECTRONIC AND VIBRATIONAL PROPERTIES

A. Electronic density of states

Fig. 16 represents the calculated electronic density of states (EDOS, Kohn-Sham energies) for the different As–Se compositions. We first observe that the calculated distribution of the valence bands is in rather good agreement with the one

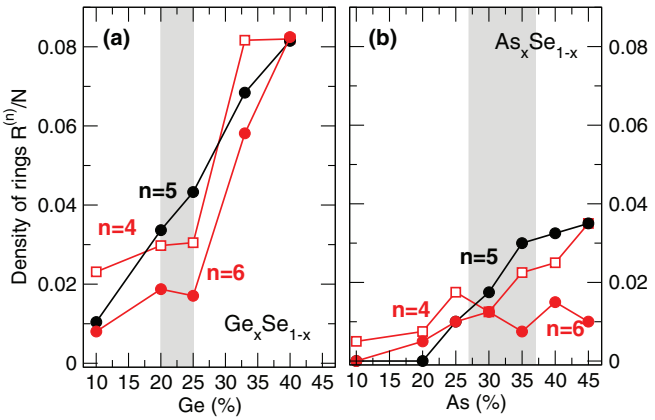

FIG. 15. Density of small rings $R^{(n)}/N$ ($3 < n < 7$) in amorphous Ge_xSe_{1-x}[152] (a) and As_xSe_{1-x} (b) as a function of modifier content x. The gray zone indicates the experimentally determined intermediate phases.[58,92,107] Here N is the number of atoms of the system.

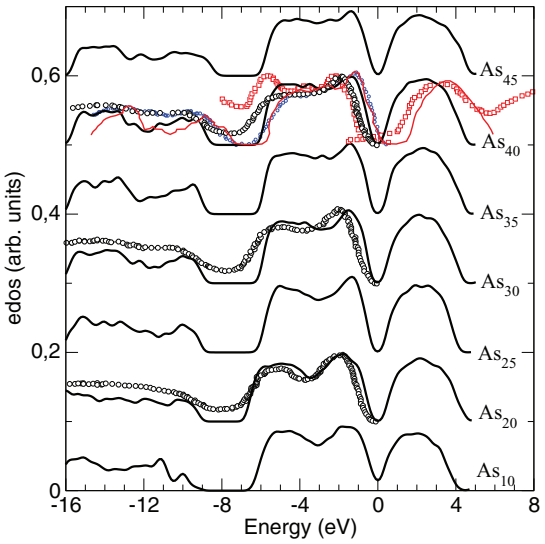

FIG. 16. Computed electronic density of states in As_xSe_{1-x} for different compositions (black lines). The results are compared to experimental measurements from (i) photoemission spectroscopy (circles,[167] filled red squares,[168] blue circles[129]) for the valence bands and (ii) inverse photoemission measurements (open red squares, Ref. 168) for the conduction band. The solid red curve is an *ab initio* simulation from Drabold and co-workers.[129] For a better comparison along the x-axis, the experimental curves have been adapted to match the valence band edge around the Fermi energy and up to the top of principal peak.

determined experimentally for different As content from x-ray photoemission spectroscopy[129,167,168] (XPS), and are also consistent with earlier *ab initio* MD simulations.[129] We find indeed an EDOS profile which contains the two (As, Se) 4s-bands between $\simeq -15$ eV and $\simeq -6$ eV (see also Fig. 17), which are well separated from the valence 4p-band structure. In contrast with previous simulation on Ge-Se glasses,[152] we note that the p-band structure is less affected by the change in composition for the present As-Se glasses. The calculation of the projection of Kohn-Sham wavefunctions onto the wavefunctions associated with the atomic species shows that the partial contribution of As and Se to the EDOS leads to contributions from Se 4p electrons to the first peak (-2 eV) of the conduction band, whereas As 4s and 4p electrons contribute to bands found between -5 eV and the Fermi energy.

For the As_2Se_3 composition, we remark that the comparison of our calculation with the previous electronic modelling of Li *et al.*[129] exhibits some differences which are mostly detectable in the conduction band. We do find the main peak at 2.3 eV, whereas in Ref. 129 the same peak is found at 3.6 eV and in increased agreement with experimental findings from inverse photoemission,[168] although a LDA is used, which is known to underestimate the gap in chalcogenides. It has furthermore to be reminded that the present simulations use GGA which is known to increase the ionicity of the bonding,[139] and should, in principle, increase the gap, given also that the Becke-LYP functional reduces the metallic character of the bonding.[53]

When the effect of As content is investigated, we find that the valence band structure of $As_{20}Se_{80}$ and $As_{30}Se_{70}$ is in excellent agreement with the most recent XPS measurement from Golovchak *et al.*,[167] in particular the minimum at

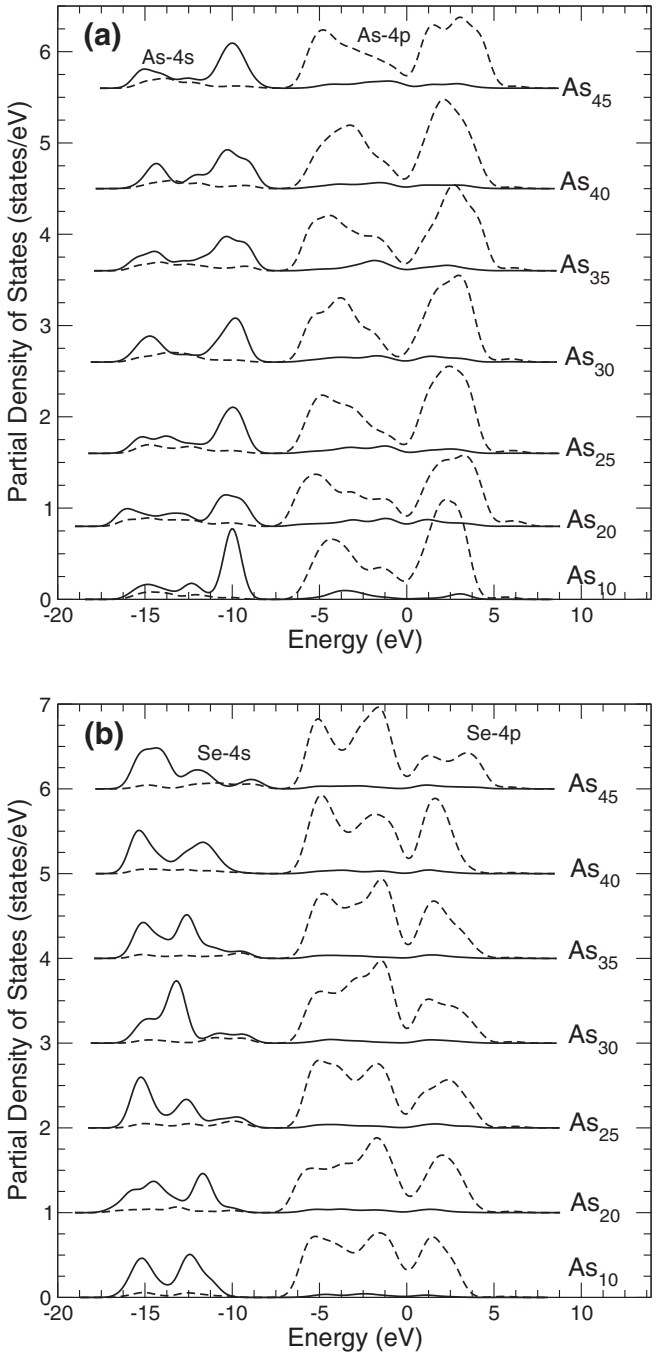

FIG. 17. Computed partial electronic density of states in As_xSe_{1-x} glasses for different compositions. Contributions from As (a) and Se (b) 4s (solid line) and 4p (broken line) electrons.

$\simeq -4.0$ eV is clearly reproduced, and an inspection of the partial EDOS (Fig. 17) shows that the minimum mostly arises from the dual contribution of both the Se-4p (at -2 eV) and Ge-4p (at -5 eV) electronic contributions. The increase of As content tends to reduce this structured band, and leads for the stoichiometric As_2Se_3 composition to a broad band between -6 eV and the Fermi energy. This situation is actually very close to the one encountered in Ge-Se.[152] However, in contrast with the latter (see also Ref. 169) no change in the conduction band is found between flexible and isostatic composition, and the calculated EDOS simply leads to a broad band between 0 and 4 eV.

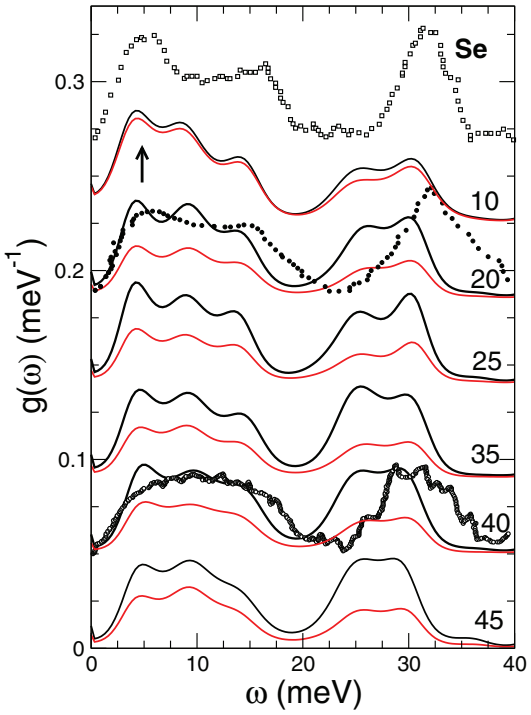

FIG. 18. Computed total vibrational density of states (VDOS) of As_xSe_{1-x} glasses (solid line) compared to available experimental measurements[171,172] (circles for x = 40% and x = 16% As). Red curves represent the partial VDOS for Se. Data for pure selenium[172] (squares) are put for comparison. The arrow indicate the floppy mode peak.

B. Vibrational properties

Figure 18 shows the total computed VDOS of As-Se glasses with changing As content. Results for the stoichiometric compound (As_2Se_3, i.e., 40% As) are compared to experimental data obtained from inelastic neutron diffraction,[171] and shows a rather good agreement as the low frequency part is reproduced up to 15-20 meV. For the As_2Se_3 compound, the VDOS consists in a first peak at 5 meV which is part of a broad band ending at 15-20 meV, and which is separated from a second band found between 22 and 32 meV. When compared to experiments, we note an important shift for the latter contribution (25-35 meV), usually attributed to bond-stretching vibrations, and also obtained in similar studies[152,170] on $GeSe_2$. The change on composition (i.e., enriching the glass with selenium) changes only moderately the high frequency contribution with a decrease of the peak signaled at 30 meV. The detail of Se contributions (red curves, Fig. 18) shows that most of the changes due to composition are embedded in the Se partial VDOS. The peak at 30 meV can be assigned to Se stretching vibrations as it is also found in the corresponding experimental VDOS for pure Se (Fig. 18) where a prominent peak is measured at $\simeq$30 meV. This peak is clearly present for the 10%–25% compositions and then decreases in intensity.

On the low frequency side, one notices that the intense peak at 5 meV obtained for the 10%–25% As compositions decreases for larger compositions, and this peak mostly arises from Se contributions as also seen from the experimental VDOS of pure selenium.[172] In experimental studies on the

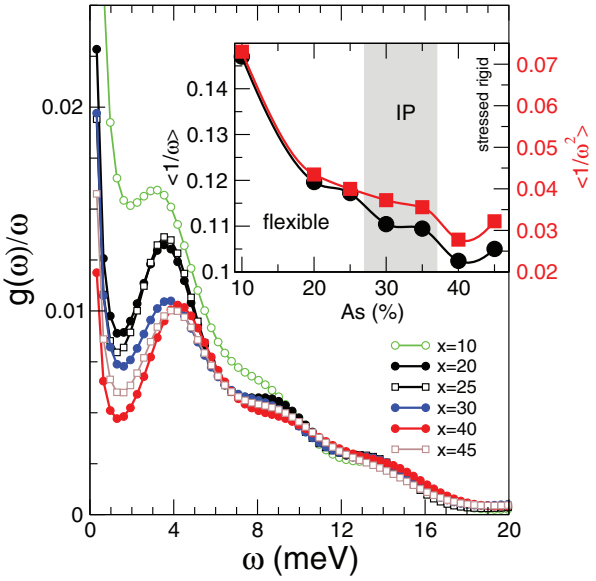

FIG. 19. Reduced VDOS $g(\omega)/\omega$ for selected compositions in As_xSe_{1-x} glasses. The inset shows the first (black symbols) and the second inverse moment (right axis, red symbols) as a function of As composition. The gray zone indicates the intermediate phase, determined experimentally.

VDOS of chalcogenide glasses (Ref. 172), this peak has been identified with the presence of floppy modes that acquire a finite energy because of the presence of residual interactions (van der Waals, dihedral), which shift the zero deformation energy of idealized networks[64,173] to a finite value (5 meV). In the present simulations, the floppy mode peak is found to reduce in intensity and to shift to higher frequencies, as seen from a reduced plot in $g(\omega)/\omega$ (Fig. 19) which emphasizes the low-frequency region. This evolution is consistent with the loss of deformation modes which are present in the flexible phase (from $As_{10}Se_{90}$ to $As_{20}Se_{80}$), and which tend to decrease as the As content is increased. However, there is no obtained threshold close to the IP, and this observation has been already made earlier[172] from inelastic neutron scattering on ternary As–Ge–Se chalcogenides. The decrease of both $\langle 1/\omega \rangle$ (a rough measure of the floppy mode intensity) and the second inverse moment ($\langle 1/\omega^2 \rangle$) reveals the progressive stiffening of the network, but no threshold behavior can be detected from the trend in composition (inset of Fig. 19).

VII. BEHAVIOR OF THE LIQUID PHASE

It is interesting to investigate the change in topology of As-Se liquids with increasing temperature since there is evidence for a breakdown in the network structure.[16]

A. Structure

We first focus on the structure of the liquids. Fig. 7 shows the calculated total pair correlation functions for different As content. Usual features are recovered such as a reduction of the intensity and a broadening of the principal peaks at $r = d_1$ and $r = d_2$. Typical correlation distances are found to be nearly identical between the amorphous phase and the 800 K liquid, as one finds for, e.g., $As_{20}Se_{80}$ a main distance at $r = 2.42$ Å, to be compared with the one (2.41 Å) measured at 673 K by Usuki *et al.*[16]

Similar observations can be made for the partial pair correlation functions which are shown (red curves) in Fig. 8 for the temperature of 800 K. It can be noticed that the obtained threshold composition found for the occurrence of homopolar As–As bonds (at 35% As) is still obtained (Fig. 8(a)), indicating that the signature for the onset of rigidity that has been detected in the amorphous phase (Fig. 10) is also visible at elevated temperatures. The extension of the notion of rigidity and constraints counting to liquids has also received support from NMR-related relaxational phenomena.[174]

B. Dynamics

In order to follow the dynamics, we first compute the mean-square displacement $\langle r^2(t) \rangle_\alpha$ of a tagged atom of type α in the melt using the definition:

$$\langle r^2(t) \rangle_\alpha = \frac{1}{N_\alpha} \sum_{i=1}^{N_\alpha} \langle |r_i(t) - r_i(0)|^2 \rangle, \tag{9}$$

where N_α is the number of atoms α. The time dependence of this quantity for the selenium atom is shown in Fig. 20(a) for the $As_{40}Se_{60}$ composition for different temperatures ranging between the ≃2000 K and the low temperature glass (300 K). As seen from the figure, a diffusive régime sets in at long times, e.g., for $t \geq 0.5$ ps for T>1200 K and for $t \geq 5$ ps at 800 K. For the lowest temperature, a cage-like motion is obtained, as detected (e.g., at 600 K) from the lowering of the mean-square displacement at intermediate times (0.5–10 ps). At such temperatures, the diffusive régime cannot be reached.

The diffusion constant D_i (i = As, Se) can be obtained using the Einstein relation limit:

$$D_\alpha = lim_{t \to \infty} \frac{\langle r^2(t) \rangle_\alpha}{6t} \tag{10}$$

and both D_{Se} and D_{As} are plotted as a function of As content for the isotherm 800 K (Fig. 20(b)). D_{Se} can also be plotted in Fig. 21 as a function of the inverse temperature in a semi-log plot, indicating that the temperature behavior is

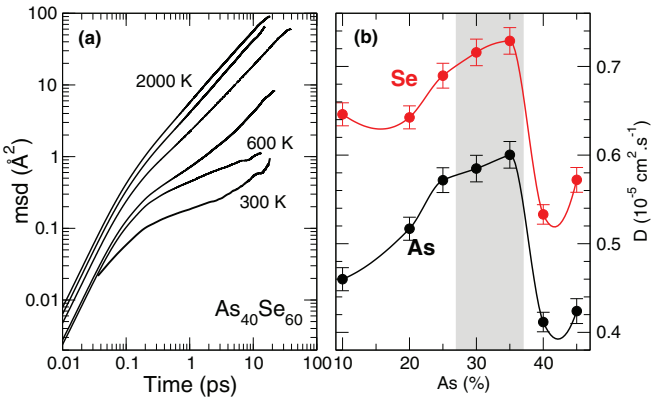

FIG. 20. (a) Mean square displacement of Se atoms for different temperatures (2000 K, 1600 K, 1200 K, 800 K, and 600 K) in liquid $As_{40}Se_{60}$. (b) Calculated As/Se diffusion constants at 800 K as a function of As content. The gray zone represents the experimentally reported IP.[58,107]

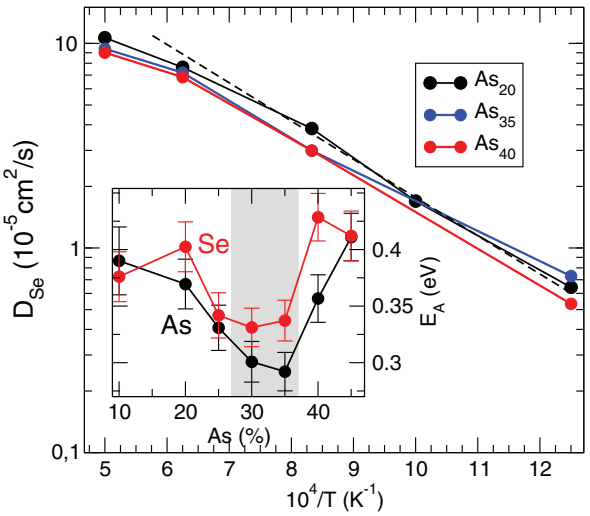

FIG. 21. Calculated Se self-diffusion constant D_{Se} as a function of inverse temperature for selected compositions in As-Se liquids. The broken line is an Arrhenius fit of $D_{Se}(T)$ and serves to extract the activation energies (inset) as a function of As content. The gray zone represents the experimentally reported IP.[58,107]

Arrhenius-like when approaching the glass transition temperature ($D_\alpha \simeq \exp[E_A/k_BT]$). Similar results are obtained for the As atoms (not shown). At high temperature, the diffusion constant departs from the Arrhenius behavior, and this has been noted earlier in other simulated strong glass-formers such as silica[175] or germania.[176]

An Arrhenius fit leads to the estimation of the activation energy E_A for diffusion that is represented as a function of As content in the inset of Fig. 21. It is found that E_A displays a minimum in the IP for 30% As, leading to energies equal to 0.29 eV and 0.34 eV for Se and As, respectively.

In addition, it is found that both species (As, Se) display a diffusivity maximum located in the same IP compositional interval (Fig. 20(b)), with a maximum value of $D_{Se} = 0.72 \times 10^{-5}$ cm^2/s for 35% As. The obtained diffusivity anomaly actually also relates to the well-known transport anomalies reported for densified tetrahedral liquids[177,178] as exemplified by the well-known example of densified water.[179]

It has been stressed[177,179] that defining local structural order parameters[180] in such dense liquids could help in understanding the relationship between diffusivity anomalies, structural, and thermodynamic anomalies under temperature and density change. One order parameter (translational) usually measures the tendency of pairs of molecules to be separated by a preferential distance, while a second order parameter (orientational) measures the tendency of a molecule and its nearest neighbours to adopt preferential orientations. As liquids are followed under density and temperature change, it has been found that diffusivity anomalies under compression, and temperature-induced space-filling tendency are deeply related to changes in the local structural order, and also to the excess entropy.[178] From the present investigated As–Se system, and from an earlier studied sodium silicate liquid,[148] one now recognizes that anomalies arise from the constraint behavior, and that stress adaptation typical of IP compositions[113–117] is the dominant feature which drives the evolution of transport coefficient under density and temperature change. We thus view these anomalies as consequences of structural rearrangements[177] driven by stress adaptation in select pressure,[148] composition (As–Se) or density windows[179] when the underlying networks are isostatic.

We finally remark that the trends in composition of dynamic properties (D_i, E_A) are correlated with those obtained in reciprocal (k_{FSDP}, Δk_{FSDP}, Fig. 6) and real space properties (in n_{AsAs}, Fig. 10). The present results highlight the fact that in a certain compositional interval found between roughly 30%–35% As, As–Se bonding favors the formation of coherent microdomains extending over intermediate range order distances ($\simeq$10 Å) as detected in reciprocal space. These domains can form due to the low activation barriers and the enhanced diffusion of the species involved. Therefore, a close link exists between unmistakable fingerprints of structural and dynamical properties in the vicinity and within the intermediate phase.

C. Van Hove correlation function

In order to provide additional insight into the anomaly obtained for the diffusivity of intermediate phase compositions at 800 K (Fig. 20), we calculate the self-part of the Van Hove correlation function defined by

$$\mathcal{G}_s^\alpha(r,t) = \frac{1}{N_\alpha}\left\langle \sum_{k=1}^{N_\alpha} \delta(r - |\mathbf{r}_k(0) - \mathbf{r}_k(t)|)\right\rangle, \qquad (11)$$

where $\delta(r)$ is the Dirac function. We remind that the self-part of the Van Hove correlation function $\mathcal{G}_s^\alpha(r,t)$ is the probability density of finding an atom α at time t knowing that this atom was at the origin ($r = 0$) at time $t = 0$. By probing the probability that an atom has moved by this distance r, one is, therefore, able to probe additional aspects of dynamics.

Fig. 22 represents the Van Hove function $4\pi r^2 \mathcal{G}_s^{Se}(r,t)$ for Se atoms at different times. Note that because of the isotropic nature of the system, the angular integration can be

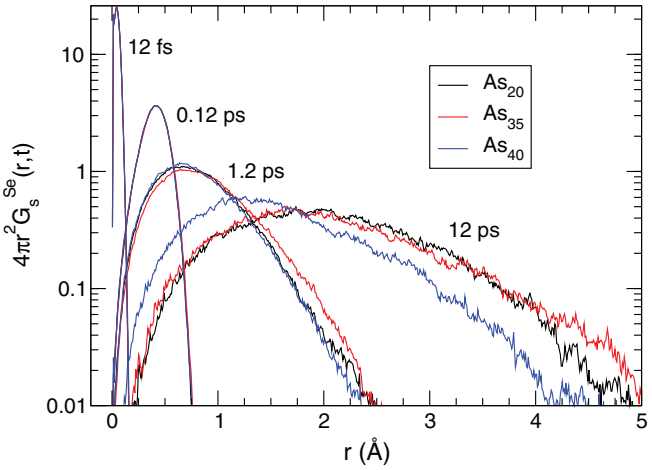

FIG. 22. Calculated self-part of the Van Hove correlation function $4\pi r^2 \mathcal{G}_s^{Se}(r,t)$ at 800 K for three selected compositions in As-Se liquids: flexible $As_{20}Se_{80}$ (black curve), intermediate $As_{35}Se_{65}$ (red curve) and $As_{40}Se_{60}$ (blue curve). The function is represented for selected times: 12 fs, 0.12 ps, 1.2 ps, 12 ps.

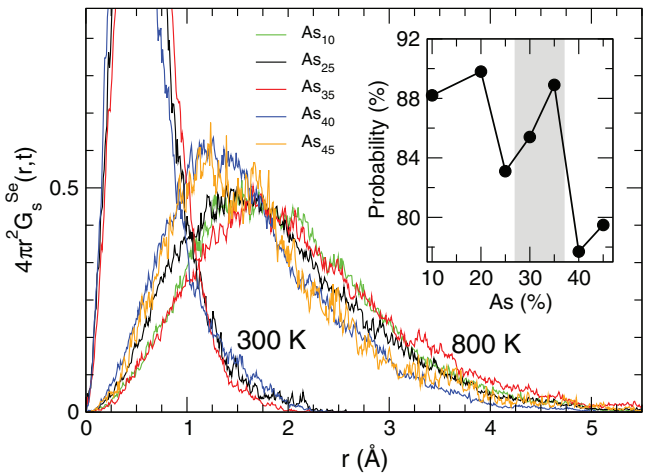

FIG. 23. Calculated self-part of the Van Hove correlation function $4\pi r^2 \mathcal{G}_s^{Se}(r,t)$ at $t = 12$ ps with varying As content, and temperature (800 K (same as Fig. 22), and 300 K). The inset shows the probability that a Se atom has jumped by 1 Å during 12 ps at 800 K, as a function of As content.

performed leading to the term $4\pi r^2$. For very short times (12 fs), $4\pi r^2 \mathcal{G}_s^{Se}(r,t)$ nearly reduces to the Dirac function as it should be.[181] For increased times however, the Se atoms now experience larger distances for a given time and for $t = 12$ ps, atoms move over distances typical of second nearest neighbor distances (4-5 Å). For the longest time, we find the behavior of $4\pi r^2 \mathcal{G}_s^{Se}(r,t)$ to be qualitatively different for the 40% As composition, when compared to intermediate (35%) or flexible (20%) compositions. In fact, distances which are sampled over 12 ps appear to be reduced from 5 Å to 4 Å. This effect is also present at T = 600 K (not shown) but nearly absent at room temperature (Fig. 23). For this lowest temperature and for the considered time scale, atoms are trapped in a cage-like dynamics leading to a plateau-like behavior for the mean-square displacement as exemplified for the lowest temperature in Fig. 20.

From these functions, we now calculate the probability that a Se atom jumped by 1 Å during a time of 12 ps at 800 K. The chosen distance corresponds to the value of the plateau-like behavior seen in the mean-square displacement for times larger than 1 ps. We find a non-monotonic trend for this jump probability, given that the probability remains first constant ($\simeq$90%) at low As content, prior to an important decrease at the flexible to intermediate boundary. This drop is followed by a steady increase for the IP compositions, followed by a sharp decrease to $\simeq$77% as the system becomes stressed rigid.

VIII. CONCLUDING REMARKS

As_xSe_{1-x} glasses not only represent the archetypal system that serve as benchmark for the detection of flexible to rigid transitions, but also display a variety of structural features and potential applications in optoelectronics. The characterization of their structural, thermal, electronic and vibrational properties remains timely despite of decades of intensive research that trace back to the pioneering work of Myers and Felty.[182] The general structural evolution is well understood and results from the progessive cross-linking of $AsSe_{3/2}$ pyramids into a basic network of Se chains that is found in elemental selenium. This ultimately leads to a fully 3D network that has been especially investigated at the stoichiometric composition As_2Se_3. Much less is known on the details of the structure and particularly on structural defects such as homopolar bondings, an issue of obvious interest for the case of non-stoichiometric chalcogenides, and coordination defects. Both are known to lead to the peculiar electronic properties of chalcogenides close to the Fermi energy. In addition, the simple cross-link picture fails to describe most of the observed non-monotonic compositional trends of physico-chemical properties such as those revealed by the evolution with As content of the non-reversing enthalpy at the glass transition, fragility, molar volume, mechanical properties, while being also unable to account for the non mean-field effects of rigidity transitions.

In the present contribution we have used FPMD simulations to investigate in detail the effect of As content on various properties by focusing on seven target compositions. These compositions belong to the previously determined elastic phases[58,107] characterized by rigidity theory: a flexible Se-rich phase which contains local deformation (floppy) modes, an As-rich phase which is stressed rigid and locked by an important bond density, and a compositional interval (the intermediate phase) in which glasses adapt in order to lower compositionally induced stress. It is important to emphasize that attempts to understand these features from molecular simulations have been reported only recently.[118,152]

The FPMD simulations are found to reproduce with an excellent accuracy the available diffraction results in both real and reciprocal space for selected As compositions: $As_{20}Se_{80}$, $As_{35}Se_{65}$, and $As_{40}Se_{60}$. The FSDP obtained at $\simeq 1$ Å^{-1} is found to be mostly due to As–Se correlations, and the parameters characterizing this peak can be investigated with composition. These reveal that anomalies in both the position k_{FSDP} and the width Δk_{FSDP} do exist in a compositional interval that corresponds to the reported intermediate phase.[58] In real space, the structure is made of structural $AsSe_{3/2}$ motifs that connect with Se chains, but FPMD allows for a more detailed picture which shows that homopolar As–As bondings appear at intermediate phase compositions. When the two opposite trends in homopolar bondings (monotonic decrease of Se–Se and threshold increase of As–As) are followed with As content, an immediate consequence is that heteropolar bonding As–Se will maximize in the intermediate phase, a feature that also leads to anomalous signatures for As–Se correlations in reciprocal space.

Having validated the accuracy of the structural models by a direct comparison with experimental structure functions, we have then determined all possible structural information that can be obtained from the simulated trajectories: coordination numbers, neighbor distributions, bond angle distributions, ring statistics. These simulations show that the octet (8-$\mathcal{N}$) rule is valid for all compositions so that the local geometry is a $AsSe_{3/2}$ pyramid with a minority of QT units (<10%). The medium range order has been also characterized from a ring analysis. In contrast with a similar chalcogenide (Ge–Se[152]), no threshold behavior is found in the ring statistics, and, in addition, the ring density is found to be substantially lower

which may suggest that the present As–Se has all the features of a dendritic glass.

What are the broader perspectives and conclusions of the present results? Studies challenging the existence of the intermediate phase have unfortunately overlooked the variety of signatures that lead to an unambiguous definition of a double threshold flexible-intermediate and intermediate-stressed rigid: thermal, calorimetric, electrical, spectroscopic, mechanical, etc. Instead, an aggressive focus has been made on the measurement of the sole non-reversing heat flow (ΔH_{nr}). For reasons which are still not elucidated, this key quantity can display with composition rather different shapes, ranging from a square well behavior that lead to well-defined threshold compositions x_{c1} and x_{c2} and obviously indicate the presence of the underlying elastic phase transitions, to a much broader behavior for certain systems, and this is obviously the case for the present As–Se (Fig. 1) which displays also other anomalies still allowing for a neat definition of IP boundaries between 27% and 37% As.[107] However, despite these obvious experimental signatures which are also found in the isochemical As–S,[83] the understanding of the origin of the IP in As–Se remains open. This system being furthermore highly sensitive to impurities, light exposure[59] and sample heterogeneity,[107] the intrinsic behavior of the elastic phase transitions can be lost in glasses of unproven homogeneity.[108]

FPMD simulations can provide insight into this topic of crucial interest in glass science, and here we have shown that a cascade of other anomalies are found in dynamic properties (diffusivity, activation energies) and structural properties. Concerning the latter, we have shown that proposed QT units cannot explain alone[58] the shift in composition of the flexible to rigid transitions, from the mean-field estimate of 40% to an IP detected between 27% and 37%. However, it is important to emphasize that these units dominate in the supercooled liquid phase, and may, thus, be important to consider in a mean-field constraint count close to the glass transition.

ACKNOWLEDGMENTS

The authors thank P. Boolchand, M. Boero, D. Skoncz-Traintz, E. Bychkov, S. Boshle, K. Gunasekera, C. Massobrio, and J. C. Phillips for useful and stimulating discussions and data sharing. Support from Agence Nationale de la Recherche (ANR) (Grant No. 09-BLAN-0109-01) is gratefully acknowledged. GENCI (Grand Equipement National de Calcul Intensif) is acknowledged for supercomputing access. MM acknowledges the Franco-American Fulbright Commission and International Materials Institute (H. Jain) for support.

[1] M. Vlek and M. Frumar, J. Non-Cryst. Solids **97–98**, 1223 (1987).
[2] L. Tichy, H. Ticha, P. Nagels, R. Callaerts, R. Mertens, and M. Vleck, Mater. Lett. **39**, 122 (1999).
[3] O. Nordman, N. Nordman, and N. Peyghambarian, J. Appl. Phys. **84**, 6055 (1998).
[4] C. Derbidge and P. C. Taylor, J. Non-Cryst. Solids **351**, 233 (2005).
[5] M. L. Trunov, V. S. Bilanich, S. N. Dub, and R. S. Shmegera, JETP Lett. **82**, 504 (2005).
[6] S. N. Yannopoulos and M. L. Trunov, Phys. Status Solidi **246**, 1773 (2009).
[7] M. L. Trunov, C. Cserhàti, P. M. Lytvyn, Y. Kaganovskii, and S. Kökényesi, J. Phys. D **46**, 245303 (2013).
[8] J. T. Edmond and M. W. Redfearn, Proc. Phys. Soc. **81**, 380 (1963).
[9] A. R. Hilton, C. E. Jones, R. D. Dobrott, H. M. Klein, A. M. Bryant, and T. D. George, Phys. Chem. Glasses **7**, 116 (1966).
[10] G. Lucovsky, Phys. Rev. B **6**, 1480 (1972).
[11] P. C. Taylor, S. G. Bishop, and D. L. Mitchell, Solid State Commun. **8**, 1783 (1970).
[12] Y. Sagara, O. Uemura, S. Okuyama, and T. Satow, Phys. Status Solidi A **31**, K33 (1975).
[13] M. Fabian, E. Sváb, V. Pamukchieva, A. Szekeres, S. Vogel, and U. Ruett, J. Phys. Condens. Matter **253**, 012053 (2010).
[14] S. Xin and P. S. Salmon, Phys. Rev. B **78**, 064207 (2008).
[15] O. Uemura, Y. Sagara, D. Muno, and T. Satow, J. Non-Cryst. Solids **30**, 155 (1978).
[16] T. Usuki, K. Itoh, Y. Kameda, and O. Uemura, Mater. Trans., JIM **39**, 1135 (1998).
[17] W. A. King, A. G. Clare, W. C. Lacourse, K. Volin, A. C. Wright, and A. J. Wanless, Phys. Chem. Glasses **38**, 269 (1997).
[18] T. Mori and T. Arai, J. Non-Cryst. Solids **59–60**, 867 (1983).
[19] A. J. Leadbetter and A. J. Apling, J. Non-Cryst. Solids **63**, 15 (1976).
[20] A. P. Sokolov, Phys. Rev. Lett. **78**, 2405 (1997).
[21] J. Notholt and J. Liese, Phys. State Solidi A **114**, 207 (1989).
[22] E. Bychkov, C. J. Benmore, and D. L. Price, Phys. Rev. B **72**, 172107 (2005).
[23] A. L. Renninger and B. L. Averbach, Phys. Rev. B **8**, 1507 (1975).
[24] S. Hosokawa, Y. Sakaguchi, and K. Tamura, J. Non-Cryst. Solids **150**, 35 (1992).
[25] G. Chen, H. Jain, M. Vlcek, J. Li, S. Khalid, and D. Drabold, J. Non-Cryst. Solids **326–327**, 257 (2003).
[26] V. Mastelaro, H. Dexpert, S. Benazeth, and R. Ollitrault-Fichet, J. Solid State Chem. **96**, 301 (1992).
[27] K. J. Rao, Pramana **16**, 309 (1981).
[28] K. Tamura, S. Hosokawa, M. Inui, M. Yao, H. Endo, and H. Hoshino, J. Non-Cryst. Solids **150**, 351 (1992).
[29] E. D. Crozier, F. W. Lytle, D. E. Sayers, and E. A. Stern, Can. J. Chem. **55**, 1968 (1977).
[30] S. Hosokawa, A. Koura, J.-F. Bérar, W. C. Pilgrim, S. Kohara, and F. Shimojo, Europhys. Lett. **102**, 66008 (2013).
[31] S. Hosokawa, Y. Wang, W.-C. Pilgrim, J.-F. Bérar, S. Mamedov, and P. Boolchand, J. Non-Cryst. Solids **352**, 1517 (2006).
[32] B. Bureau, J. Troles, M. Le Floch, F. Smektala, and J. Lucas, J. Non-Cryst. Solids **326–327**, 58 (2003).
[33] B. Bureau, J. Troles, M. Le Floch, F. Smektala, G. Silly, and J. Lucas, Solid State Sci. **5**, 219 (2003).
[34] C. Rosenhahn, S. E. Hayes, B. Rosenhahn, and H. Eckert, J. Non-Cryst. Solids **284**, 1 (2001).
[35] K. Sykina, G. Yang, C. Roiland, L. Le Pollès, E. Le Fur, C. J. Pickard, B. Bureau, and E. Furet, Phys. Chem. Chem. Phys. **15**, 6284 (2013).
[36] V. Kovanda, M. Vlcek, and H. Jain, J. Non-Cryst. Solids **326–327**, 88 (2003).
[37] G. Lucovsky, F. L. Galeener, R. H. Geils, and R. C. Keezer, in *The Structure of Non-Crystalline Materials*, edited by P. H. Gaskell (Taylor & Francis, New York, 1977).
[38] T. Mori, S. Onari, and A. Arai, Jpn. J. Appl. Phys. **19**, 1027 (1980).
[39] J. Schottmiller, M. Tabak, G. Lucovsky, and A. Ward, J. Non-Cryst. Solids **4**, 80 (1970).
[40] S. Onari, K. Matsuishi, and A. Arai, J. Non-Cryst. Solids **86**, 22 (1986).
[41] J. Holubova, Z. Cernosek, and E. Cernoskova, J. Optoelectron. Adv. Mater. **9**, 1979 (2007).
[42] S. N. Yannopoulos and K. S. Andrikopoulos, Phys. Rev. B **69**, 144206 (2004).
[43] S. N. Yannopoulos and K. S. Andrikopoulos, J. Chem. Phys. **121**, 4747 (2004).
[44] V. I. Mikla, A. A. Baganich, A. P. Sokolov, and A. P. Shebanin, Phys. State Solidi B **175**, 281 (1993).
[45] R. Golovchak, J. Oelgoetz, M. Vlcek, A. Esposito, A. Saiter, J.-M. Saiter, and H. Jain, J. Chem. Phys. **140**, 054505 (2014).
[46] O. Kostadinova, Ph.D. thesis, University of Patras, 2009.
[47] R. Mohan and K. J. Rao, Proc. Indian Acad. Sci. **90**, 83 (1981).
[48] R. Mohan and K. J. Rao, Proc. Indian Acad. Sci. **90**, 229 (1981).
[49] C. T. Moynihan, P. B. Macedo, M. S. Maklad, R. K. Mohr, and R. E. Howard, J. Non-Cryst. Solids **17**, 369 (1975).
[50] L. Baidakov, Izv. Akad. Nauk. SSR Neorg. Mater. **6**, 2106 (1970).
[51] I. Petri, P. S. Salmon, and H. E. Fischer, Phys. Rev. Lett. **84**, 2413 (2000).
[52] C. Massobrio and A. Pasquarello, Phys. Rev. B **77**, 144207 (2008).

[53] M. Micoulaut, R. Vuilleumier, and C. Massobrio, Phys. Rev. B **79**, 214204 (2009).
[54] M. Bauchy and M. Micoulaut, J. Non-Cryst. Solids **377**, 34 (2013).
[55] M. Bauchy, M. Micoulaut, M. Boero, and C. Massobrio, Phys. Rev. Lett. **110**, 165501 (2013).
[56] N. Morimoto, Mineral. J. **1**, 160 (1954).
[57] T. Ito, N. Morimoto, and R. Sadanaga, Acta Crystallogr. **5**, 775 (1952).
[58] D. G. Georgiev, P. Boolchand, and M. Micoulaut, Phys. Rev. B **62**, R9228 (2000).
[59] P. Chen, P. Boolchand, and D. G. Georgiev, J. Phys. Condens. Matter **22**, 065104 (2010).
[60] *Rigidity Theory and Applications*, edited by M. F. Thorpe and P. M. Duxbury (Kluwer Academic/Plenum Publishers, New York, 1999).
[61] *Phase Transitions and Self-organization in Electronic and Molecular Networks*, edited by M. F. Thorpe and J. C. Phillips (Kluwer Academic/Plenum Publishers, New York, 2001).
[62] *Insulating and Semi-Conducting Glasses*, edited by P. Boolchand (World Scientific, Singapore, 2000).
[63] J. C. Phillips, J. Non-Cryst. Solids **34**, 155 (1979).
[64] M. F. Thorpe, J. Non-Cryst. Solids **57**, 355 (1983).
[65] J. C. Phillips, Phys. Today **35**(2), 27 (1982).
[66] V. V. Tarasov, V. M. Zhdanov, S. A. Dembovskii, and A. K. Mal'tsev, Russ. J. Appl. Chem. **42**, 1122 (1968).
[67] S. O. Kasap, D. Tonchev, and T. Wagner, J. Mater. Sci. Lett. **17**, 1809 (1998).
[68] J. Holubovà, Z. Cernosek, and E. Cernoskovà, J. Non-Cryst. Solids **355**, 2050 (2009).
[69] A. A. Elabbar and A. A. Abu-Sehly, Physica B **406**, 4261 (2011).
[70] P. C. Anderson, U. Senapati, and A. K. Vasrhneya, J. Non-Cryst. Solids **176**, 51 (1994).
[71] R. Golovchak, H. Jain, O. Spotyuk, A. Kozdras, A. Saiter, and J.-M. Saiter, Phys. Rev. B **78**, 014202 (2008).
[72] R. Golovchak, A. Kozdras, V. Balitska, and O. Spotyuk, J. Phys. Condens. Matter **24**, 505106 (2012).
[73] A. P. Chernov, S. A. Dembovskii, and S. F. Chistov, Izv. Akad. Nauk. USSR Neorg. Mater. **4**, 1658 (1968).
[74] G. Yang, T. Rouxel, J. Troles, B. Bureau, C. Boussard-Plédel, P. Houizot, and J.-C. Sangleboeuf, J. Am. Ceram. Soc. **94**, 2408 (2011).
[75] C. T. Hach, K. Cerqua-Richardson, J. P. Varner, and W. C. La Course, J. Non-Cryst. Solids **209**, 159 (1997).
[76] K. N. Madhusoodanan and J. Philip, Phys. Rev. B **39**, 7922 (1989).
[77] K. N. Madhusoodanan and J. Philip, Pramana J. Phys. **33**, 705 (1989).
[78] S. V. Nemilov and G. Petrovskii, Bull. Akad. Sci. USSR Phys. Ser. **28**, 1184 (1964).
[79] B. T. Kolomeits and V. P. Pozdnev, Sov. Phys. Solid State **2**, 23 (1960).
[80] M. Tatsumisago, B. L. Halfpap, J. L. Green, S. M. Lindsay, and C. A. Angell, Phys. Rev. Lett. **64**, 1549 (1990).
[81] J. D. Musgraves, P. Wachtel, S. Novak, J. Wilkinson, and K. Richardson, J. Appl. Phys. **110**, 063503 (2011).
[82] G. Yang, O. Gulbiten, Y. Gueguen, B. Bureau, J.-C. Sangleboeuf, C. Roiland, E. A. King, and P. Lucas, Phys. Rev. B **82**, 195206 (2010).
[83] P. Chen, C. Holbrook, P. Boolchand, D. G. Georgiev, and M. Micoulaut, Phys. Rev. B **78**, 224208 (2008).
[84] F. Wang, S. Mamedov, P. Boolchand, B. Goodman, and M. Chandrasekhar, Phys. Rev. B **71**, 174201 (2005).
[85] S. Chakravarty, D. G. Georgiev, P. Boolchand, and M. Micoulaut, J. Phys. Condens. Mater. **17**, L7 (2005).
[86] D. Selvanathan, W. J. Bresser, and P. Boolchand, Phys. Rev. B **61**, 15061 (2000).
[87] P. Boolchand, D. G. Georgiev, and B. Goodman, J. Optoelectron. Adv. Mater. **3**, 703 (2001).
[88] K. Trachenko and M. T. Dove, Phys. Rev. B **67**, 212203 (2003).
[89] S. Chakraborty and P. Boolchand, J. Phys. Chem. B **118**, 2249 (2014).
[90] S. Chakraborty, P. Boolchand, M. Malki, and M. Micoulaut, J. Chem. Phys. **140**, 014503 (2014).
[91] M. Micoulaut and M. Malki, Phys. Rev. Lett. **105**, 235504 (2010).
[92] S. Bhosle, P. Boolchand, M. Micoulaut, and C. Massobrio, Solid State Commun. **151**, 1851 (2011).
[93] C. Bourgel, M. Micoulaut, M. Malki, and P. Simon, Phys. Rev. B **79**, 024201 (2009).
[94] R. Rompicharla, D. I. Novita, P. Chen, P. Boolchand, M. Micoulaut, and W. Huff, J. Phys. Condens. Matter **20**, 202101 (2008).
[95] M. Micoulaut, J. Phys. Condens. Matter **22**, 285101 (2010).
[96] K. Gunasekara, S. Bhosle, P. Boolchand, and M. Micoulaut, J. Chem. Phys. **139**, 164511 (2013).
[97] Y. Vaills, T. Qu, M. Micoulaut, F. Chaimbault, and P. Boolchand, J. Phys. Condens. Mater. **17**, 4889 (2005).
[98] M. Micoulaut, M. Malki, D. I. Novita, and P. Boolchand, Phys. Rev. B **80**, 184205 (2009).
[99] M. Micoulaut, Am. Mineral. **93**, 1732 (2008).
[100] K. Trachenko, M. T. Dove, V. Brazhkin, and F. S. El'kin, Phys. Rev. Lett. **93**, 135502 (2004).
[101] M. Anbarasu and S. Asokan, J. Phys. D **40**, 7515 (2007).
[102] M. Anbarasu, K. K. Singh, and S. Asokan, Philos. Mag. **88**, 599 (2008).
[103] C. Das, M. S. R. N. Kiran, A. Ramamurty, and S. Asoka, Solid State Commun. **152**, 2181 (2012).
[104] D. J. Jacobs, A. J. Rader, L. A. Kuhn, and M. F. Thorpe, Proteins **44**, 150 (2001).
[105] S. W. King *et al.*, J. Non-Cryst. Solids **379**, 67 (2013).
[106] D. G. Georgiev, P. Boolchand, and M. Micoulaut, J. Optoelectron. Adv. Mater. **4**, 823 (2002).
[107] S. Ravindren, K. Gunasekera, Z. Tucker, A. Diebold, P. Boolchand, and M. Micoulaut, J. Chem. Phys. **140**, 134501 (2014).
[108] R. Bhageria, K. Gunasekera, P. Boolchand, and M. Micoulaut, Phys. State Solidi B **251**, 1322 (2014).
[109] S. Bhosle, K. Gunasekera, P. Boolchand, and M. Micoulaut, Int. J. Appl. Glass Sci. **3**, 205 (2012).
[110] S. Bhosle, K. Gunasekera, P. Boolchand, and M. Micoulaut, Int. J. Appl. Glass Sci. **3**, 189 (2012).
[111] P. Lucas, E. A. King, O. Gulbiten, J. L. Yarger, E. Soiganrd, and B. Bureau, Phys. Rev. B **80**, 214114 (2009).
[112] O. Shpotyuk and R. Golovchak, Phys. State Solidi C **8**, 2572 (2011).
[113] M. Micoulaut and J. C. Phillips, Phys. Rev. B **67**, 104204 (2003).
[114] J. Barré, A. R. Bishop, T. Lookman, and A. Saxena, Phys. Rev. Lett. **94**, 208701 (2005).
[115] M. Micoulaut, Phys. Rev. B **74**, 184208 (2006).
[116] M. V. Chubynsky, M. A. Brière, and N. Mousseau, Phys. Rev. E **74**, 016116 (2006).
[117] M. F. Thorpe, D. J. Jacobs, M. V. Chubynsky, and J. C. Phillips, J. Non-Cryst. Solids **266–269**, 859 (2000).
[118] F. Inam, G. Chen, D. N. Tafen, and D. A. Drabold, Phys. State Solid B **246**, 1849 (2009).
[119] *Rigidity and Boolchand Phases in Nanomaterials*, edited by M. Micoulaut and M. Popescu (INOE Publishing House, Bucharest, 2009).
[120] D. G. Georgiev, M. Mitkova, P. Boolchand, G. Brunklaus, H. Eckert, and M. Micoulaut, Phys. Rev. B **64**, 134204 (2001).
[121] E. Diemann, Rev. Chim. Miner. **16**, 237 (1981).
[122] T. Wagner and S. O. Kasap, Philos. Mag. B **74**, 667 (1996).
[123] E. Ahn, G. A. Williams, and P. C. Taylor, Phys. Rev. B **74**, 174206 (2006).
[124] O. Luksha, V. Ivantsky, and S. Kolinko, J. Non-Cryst. Solids **136**, 43 (1991).
[125] M. Bauchy, J. Non-Cryst. Solids **377**, 39 (2013).
[126] J. C. Mauro and A. K. Varshneya, J. Non-Cryst. Solids **353**, 1226 (2007).
[127] S. Hosokawa, Y. Kawakita, W.-C. Pilgrim, and F. Hensel, J. Non-Cryst. Solids **293–295**, 153 (2001).
[128] J. Li and D. A. Drabold, Phys. Rev. B **64**, 104206 (2001).
[129] J. Li, D. A. Drabold, S. Krishnaswami, G. Chen, and H. Jain, Phys. Rev. Lett. **88**, 046803 (2002).
[130] D. A. Drabold, J. Li, and De Nyago Tafen, J. Phys. Condens. Matter **15**, S1529 (2003).
[131] J. Li and D. A. Drabold, Phys. Rev. B **61**, 11998 (2000).
[132] K. Antoine, J. Li, D. A. Drabold, and H. Jain, J. Non-Cryst. Solids **326**, 248 (2003).
[133] J. Li and D. A. Drabold, Phys. Rev. Lett. **85**, 2785 (2000).
[134] G. Chen, H. Jain, S. Khalid, J. Li, D. A. Drabold, and S. R. Elliott, Solid State Commun. **120**, 149 (2001).
[135] F. Shimojo, S. Munejiri, K. Hoshino, and Y. Zempo, J. Phys. Condens. Matter **12**, 6161 (2000).
[136] X. F. Zhou and L. F. Chen, Physica B **403**, 3302 (2008).
[137] CPMD, http://www.cpmd.org, Copyrright IBM Corp 1990-2013, Copyright MPI für Festkörperforschung, Stuttgart 1997–2001.
[138] R. Car and M. Parrinello, Phys. Rev. Lett. **55**, 2471 (1985).
[139] C. Massobrio, A. Pasquarello, and R. Car, J. Am. Chem. Soc. **121**, 2943 (1999).
[140] C. Massobrio, M. Micoulaut, and P. S. Salmon, Solid State Sci. **12**, 199 (2010).
[141] A. D. Becke, Phys. Rev. A **38**, 3098 (1988).

[142]C. Lee, W. Yang, and R. G. Parr, Phys. Rev. B **37**, 785 (1988).
[143]L. Giacomazzi, C. Massobrio, and A. Pasquarello, J. Phys. Condens. Matter **23**, 295401 (2011).
[144]M. Kibalchenko, J. R. Yates, C. Massobrio, and A. Pasquarello, Phys. Rev. B **82**, 020202 (2010).
[145]We relate the position r of a peak in real space to the position k of a corresponding peak in Fourier space by using the relation $k \cdot r \approx 7.7$, which identifies the location of the first maximum of the spherical Bessel function $j_0(kr)$. See P. S. Salmon, Proc. R. Soc. London, Ser. A **445**, 351 (1994).
[146]P. Scherrer, Göttinger Nachricht. Gesell. **2**, 98 (1918); A. Patterson, Phys. Rev. **56**, 978 (1939).
[147]M. Micoulaut and M. Bauchy, Phys. Status Solidi B **250**, 976 (2013).
[148]M. Bauchy and M. Micoulaut, Phys. Rev. Lett. **110**, 095501 (2013).
[149]M. T. M. Shatnawi, C. L. Farrow, P. Chen, P. Boolchand, A. Sartbaeva, M. F. Thorpe, and S. J. L. Billinge, Phys. Rev. B **77**, 094134 (2008).
[150]D. Caprion and H. Schober, Phys. Rev. B **62**, 3709 (2000).
[151]R. Kaplow, T. A. Rowe, and B. L. Averbach, Phys. Rev. B **168**, 1068 (1968).
[152]M. Micoulaut, A. Kachmar, M. Bauchy, S. Le Roux, C. Massobrio, and M. Boero, Phys. Rev. B **88**, 054203 (2013).
[153]M. Bauchy and M. Micoulaut, J. Non-Cryst. Solids **357**, 2530 (2011).
[154]M. Bauchy, M. Micoulaut, M. Celino, M. Boero, S. Le Roux, and C. Massobrio, Phys. Rev. B **83**, 054201 (2011).
[155]M. Micoulaut, C. Otjacques, J.-Y. Raty, and C. Bichara, Phys. Rev. B **81**, 174206 (2010).
[156]S. R. Elliott, *The Physics of Amorphous Materials* (Longman, Harlow, 1990).
[157]K. S. Liang, A. Bienenstock, and C. W. Bates, Phys. Rev. B **10**, 1528 (1974).
[158]J. Dixmier and R. Mosseri, J. Phys. Lett. **41**, 5 (1980).
[159]R. M. White, J. Non-Cryst. Solids **16**, 387 (1974).
[160]M. G. Fee, and H. J. Trodhal, in *Disordered Semiconductors*, edited by M. A. Kastner, G. A. Thomas, and S. R. Ovshinsky (Plenum Press, New York, 1987), p. 307.
[161]V. King, Nature (London) **213**, 1112 (1967).
[162]D. S. Franzblau, Phys. Rev. B **44**, 4925 (1991).
[163]S. Le Roux and P. Jund, Comput. Mater. Sci. **49**, 70 (2010); **50**, 1217 (2011).
[164]X. Yuan and A. N. Cormack, Comput. Mater. Sci. **24**, 343 (2002).
[165]M. Micoulaut, X. Yuan, and L. W. Hobbs, J. Non-Cryst. Solids **353**, 1951 (2007).
[166]J. Akola and R. O. Jones, Phys. Rev. B **76**, 235201 (2007).
[167]R. Golovchak, A. Kovalsky, A. C. Miller, H. Jain, and O. Spotyuk, Phys. Rev. B **76**, 125208 (2007).
[168]S. Hosokawa, A. Goldbach, M. Boll, and F. Hensel, Phys. State Solidi B **215**, 785 (1999).
[169]M. Taniguchi, T. Kouchi, I. Ono, S. Hosokawa, M. Nakatake, H. Namatame, and K. Murase, J. Electron Spectrosc. Relat. Phenom. **78**, 507 (1996).
[170]M. Cobb, D. A. Drabold, and R. L. Cappelletti, Phys. Rev. B **54**, 12162 (1996).
[171]B. Effey and R. L. Cappelletti, Phys. Rev. B **59**, 4119 (1999).
[172]W. A. Kamitakahara, R. L. Cappelletti, P. Boolchand, B. Halfpap, F. Gompf, D. A. Neumann, and H. Mutka, Phys. Rev. B **44**, 94 (1991).
[173]H. He and M. F. Thorpe, Phys. Rev. Lett. **54**, 2107 (1985).
[174]E. L. Gjersing, S. Sen, and R. E. Youngman, Phys. Rev. B **82**, 014203 (2010).
[175]J. Horbach and W. Kob, Phys. Rev. B **60**, 3169 (1999).
[176]M. Micoulaut, Y. Guissani, and B. Guillot, Phys. Rev. E **73**, 031504 (2006).
[177]M. Scott Shell, P. G. Debenedetti, and A. Z. Panagiotopoulos, Phys. Rev. E **66**, 011202 (2002).
[178]B. Shadrack Jabes, M. Agarwal, and C. Chaktavarty, J. Chem. Phys. **132**, 234507 (2010).
[179]J. R. Errington and P. G. Debenedetti, Nature **409**, 318 (2001).
[180]P. L. Chau and A. J. Hardwick, Mol. Phys. **93**, 511 (1998).
[181]J. P. Hansen, Mc Donald, *Theory of Simple Liquids* (Academic Press, New York, 1986).
[182]M. B. Myers and E. J. Felty, MRS Bull. **2**, 535 (1967).